nature medicine

Monolayered mesenchymal stem cells repair scarred myocardium after myocardial infarction

Yoshinori Miyahara[1,9], Noritoshi Nagaya[1,9], Masaharu Kataoka[1], Bobby Yanagawa[1], Koichi Tanaka[1], Hiroyuki Hao[2], Kozo Ishino[3], Hideyuki Ishida[4], Tatsuya Shimizu[5], Kenji Kangawa[6], Shunji Sano[3], Teruo Okano[5], Soichiro Kitamura[7] & Hidezo Mori[8]

Mesenchymal stem cells are multipotent cells that can differentiate into cardiomyocytes and vascular endothelial cells. Here we show, using cell sheet technology, that monolayered mesenchymal stem cells have multipotent and self-propagating properties after transplantation into infarcted rat hearts. We cultured adipose tissue–derived mesenchymal stem cells characterized by flow cytometry using temperature-responsive culture dishes. Four weeks after coronary ligation, we transplanted the monolayered mesenchymal stem cells onto the scarred myocardium. After transplantation, the engrafted sheet gradually grew to form a thick stratum that included newly formed vessels, undifferentiated cells and few cardiomyocytes. The mesenchymal stem cell sheet also acted through paracrine pathways to trigger angiogenesis. Unlike a fibroblast cell sheet, the monolayered mesenchymal stem cells reversed wall thinning in the scar area and improved cardiac function in rats with myocardial infarction. Thus, transplantation of monolayered mesenchymal stem cells may be a new therapeutic strategy for cardiac tissue regeneration.

Myocardial infarction, a main cause of heart failure, leads to loss of cardiac tissue and impairment of left ventricular function. Therefore, restoring the scarred myocardium is desirable for the treatment of heart failure. Although needle injections of bone marrow cells into the myocardium have been performed for cardiac regeneration[1–5], it is difficult to reconstruct sufficient cardiac mass in the thinned scar area after myocardial infarction.

Recently, our colleagues have developed cell sheets using temperature-responsive culture dishes[6]. These cell sheets allow for cell-to-cell connections and maintain the presence of adhesion proteins because enzymatic digestion is not needed[7–10]. Therefore, cell sheet transplantation may be a promising strategy for partial cardiac tissue reconstruction. Skeletal myoblasts, fetal cardiomyocytes and embryonic stem cells have been considered as candidates for an implantable cell source[11–13]. It is difficult, however, to produce a multilayered construct requiring a vascular network. Thus, autologous somatic stem cells with self-propagating properties that can induce angiogenesis are a desirable cell source for a transplantable sheet.

Mesenchymal stem cells (MSCs) are multipotent adult stem cells that reside within the bone marrow microenvironment[14,15]. MSCs can differentiate not only into osteoblasts, chondrocytes, neurons and skeletal muscle cells, but also into vascular endothelial cells[16] and cardiomyocytes[17–20]. In contrast to their hematopoietic counterparts, MSCs are adherent and can expand in culture. Recently, MSCs have been isolated from adipose tissue[21–24], which is typically abundant in individuals with cardiovascular disease. Here, we investigated the therapeutic potency of monolayered MSCs derived from adipose tissue using cell sheet technology.

RESULTS

Characteristics of adipose tissue–derived MSCs

We isolated MSCs from subcutaneous adipose tissue of male Sprague-Dawley rats on the basis of the adherent properties of these cells. We obtained $1.7 \times 10^5 \pm 0.2 \times 10^5$ cells from 1 g adipose tissue in a 12-h culture. By day 4 of culture of the minced adipose tissue, spindle-shaped adherent cells were apparent and formed symmetric colonies. After approximately three to four passages, most adherent cells expressed CD29 and CD90 (**Supplementary Fig. 1** online). In contrast, the majority of adherent cells were negative for CD34 and CD45. They were also negative for CD31, a marker for vascular endothelial cells, and negative for α smooth muscle actin (αSMA), a marker for smooth muscle cells. A small fraction of adherent cells expressed CD71, CD106 and CD117. These results were similar to those from bone marrow–derived MSCs[15,22,25] (**Supplementary Fig. 1** online). Using previously described methods[16,22,26], we confirmed that these adipose-derived adherent cells, like bone marrow–derived MSCs, were multipotent, as judged by their ability to differentiate into adipocytes, osteoblasts and vascular endothelial cells. Thus, we

[1]Department of Regenerative Medicine and Tissue Engineering, National Cardiovascular Center Research Institute and [2]Department of Pathology, National Cardiovascular Center, 5-7-1 Fujishirodai, Suita, Osaka, 565-8565, Japan. [3]Department of Cardiovascular Surgery, Okayama University Graduate School of Medicine, Dentistry and Pharmaceutical Sciences, 2-5-1 Shikata-cho, Okayama, 700-8555, Japan. [4]Department of Physiology, School of Medicine, Tokai University, Bohseidai, Isehara, Kanagawa, 259-1193, Japan. [5]Institute of Advanced Biomedical Engineering and Science, Tokyo Woman's Medical University, 8-1 Kawada-cho, Shinjuku-ku, Tokyo, 162-8666, Japan. [6]Department of Biochemistry, National Cardiovascular Center Research Institute and [7]Department of Cardiovascular Surgery, National Cardiovascular Center and [8]Department of Cardiac Physiology, National Cardiovascular Center Research Institute, 5-7-1 Fujishirodai, Suita, Osaka, 565-8565, Japan. [9]These authors contributed equally to this work. Correspondence should be addressed to N.N. (nnagaya@ri.ncvc.go.jp) or H.M. (hidemori@ri.ncvc.go.jp).

Received 9 August 2005; accepted 3 March 2006; published online 2 April 2006; doi:10.1038/nm1391

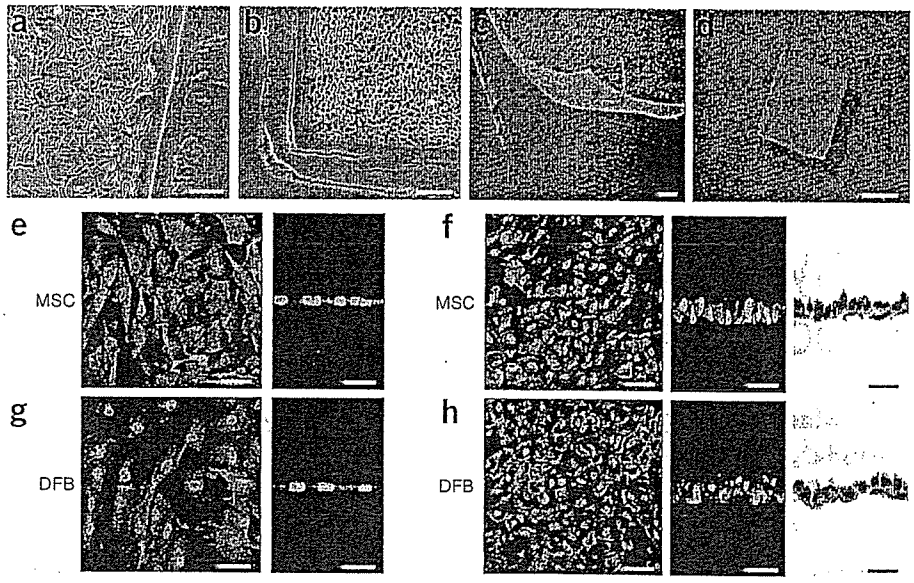

Figure 1 Preparation of monolayered MSCs. (a) MSCs 2 d after seeding on a temperature-responsive dish. (b) Cultured MSCs expanded to confluence within the square area of the dish by day 3. (c) The monolayered MSCs detached easily from the culture dish at 20 °C. (d) The completely detached monolayered MSCs were identified as a 12 × 12 mm square sheet. (e–h) Cross-sectional analysis of GFP-expressing monolayered MSCs and DFBs before detachment (e and g, confocal images) and after detachment (f and h, left and center, confocal images; right, Masson trichrome). The thickness of both monolayers was 3.5-fold greater than the thickness before detachment, and constituent cells were compacted. Scale bars in a–c, 100 μm; in d, 5 mm; in e–h, 20 μm.

confirmed that the majority of adherent cells isolated from adipose tissue were MSCs.

Preparation and transplantation of monolayered MSCs

We cultured adipose tissue–derived MSCs (5×10^5 cells) on temperature-responsive dishes for 3 d until confluent. MSCs were attached on the poly-*N*-isopropylacrylamide (PIPAAm)-grafted area (24 × 24 mm; **Fig. 1a,b**). As the culture temperature was decreased from 37 °C to 20 °C, MSCs detached spontaneously and floated up into the culture medium as a monolayer of MSCs within 40 min (**Fig. 1c,d**). As a control, we prepared dermal fibroblasts (DFBs) by the skin explant technique[27]. DFBs (8×10^5 cells) were cultured on the temperature-responsive dishes, and monolayered DFBs were fabricated as described above. The final cell counts for monolayered MSCs and DFBs before transplantation were $9.4 \pm 0.6 \times 10^5$ and $8.6 \pm 0.6 \times 10^5$ cells, respectively ($n = 6$ each). To identify the thickness of monolayered MSCs, we used green fluorescent protein (GFP)-expressing cell grafts derived from the GFP-transgenic Sprague-Dawley rats. Immediately after detachment, cells became compacted, possibly owing to cytoskeletal tensile reorganization, and the thickness of monolayered MSCs and DFBs was approximately 3.5-fold greater than the thickness before detachment (MSCs, 6.2 ± 0.3 to 21.5 ± 0.8 μm; DFBs, 6.5 ± 0.4 to 22.4 ± 1.1 μm; **Fig. 1e–h**). MSCs on the temperature-responsive dishes were positive for vimentin and slightly positive for collagen type 1, whereas DFBs were positive for both markers (**Fig. 2a**). We transferred detached monolayered MSCs above the myocardial scar (**Fig. 2b**) and then attached them to the surface of the anterior scar (**Fig. 2c**).

Secretion of angiogenic factors from monolayered MSCs

We measured secretion of angiogenic factors from MSCs 24 h after monolayers had formed, equivalent to day 4 after initial cell seeding. The monolayered MSCs secreted significantly larger amounts of angiogenic and antiapoptotic factors such as vascular endothelial growth factor (VEGF) and hepatocyte growth factor (HGF) than did the monolayered DFBs ($P < 0.01$; **Fig. 2d**). The control medium supplemented with 10% fetal calf serum contained less than 5 pg/ml of VEGF or HGF. These results suggest that the paracrine effects of monolayered MSCs on host myocardium are greater than those of monolayered DFBs.

Engraftment and growth of monolayered MSCs

To identify the transplanted cells in myocardial sections, we used GFP-expressing cell grafts derived from the GFP-transgenic Sprague-Dawley rats. We grafted monolayered MSCs or DFBs onto the scar area of the anterior wall (**Fig. 3**). Fluorescence microscopy showed that GFP-expressing monolayered MSCs gradually grew *in situ* and developed into a thick stratum, up to ~600 μm thick over the native tissue at 4 weeks (**Fig. 3a–f**). The engrafted MSC tissue tapered off toward the healthy myocardium (**Fig. 3d,e**), although most of the monolayered MSCs were attached only to the scar area in the anterior wall because of the large infarct. We rarely detected TUNEL-positive MSCs in the sheet (<1%) 48 h after transplantation (**Fig. 3g**), implying that cell viability in the sheet was maintained. In contrast, we frequently detected TUNEL-positive cells (15% ± 2%) in the DFB sheet, which was observed as a thin layer above the scar. Subsequently, the DFB sheet was undetectable 1 week later. Masson trichrome staining showed increased thickness of the anterior wall and attenuation of left ventricle enlargement after transplantation of monolayered MSCs (**Fig. 3h**), although the infarct size did not differ significantly among the untreated, DFB and MSC groups (**Supplementary Table 1** online).

Reconstruction of cardiac mass

After growth *in situ*, GFP-expressing MSC tissue contained a number of mature vascular structures that had positive staining for von Willebrand factor (vWF) and αSMA (**Fig. 4a,b**). A small fraction of the MSC tissue had positive staining for cardiac troponin T and desmin (**Fig. 4c,d**). On the other hand, a large proportion of the MSC tissue was positive for vimentin, a marker for mesenchymal lineage cells (**Fig. 4e**). The percentages of graft-derived cells that expressed endothelial (vWF), smooth muscle (αSMA), cardiac (troponin T) and mesenchymal (vimentin) markers were 12.2% ± 0.6%, 5.0% ± 0.3%, 5.3% ± 0.3% and 57.8% ± 2.2%, respectively. Notably, based on expression of these markers, two-thirds of vascular endothelial cells, four-fifths of smooth muscle cells and one-twentieth of cardiomyocytes within the MSC tissue were GFP^- and hence were derived from the host. The MSC tissue stained modestly for collagen type 1 (**Fig. 4f**). Picrosirius red staining showed that collagen deposition was found mainly in the extracellular matrix and the epicardial margin of the MSC tissue (**Fig. 4g**). Excluding staining in blood vessels, the MSC tissue was also negative for αSMA, a marker for myofibroblasts (**Fig. 4b**). This phenotype was consistent with properties of MSCs

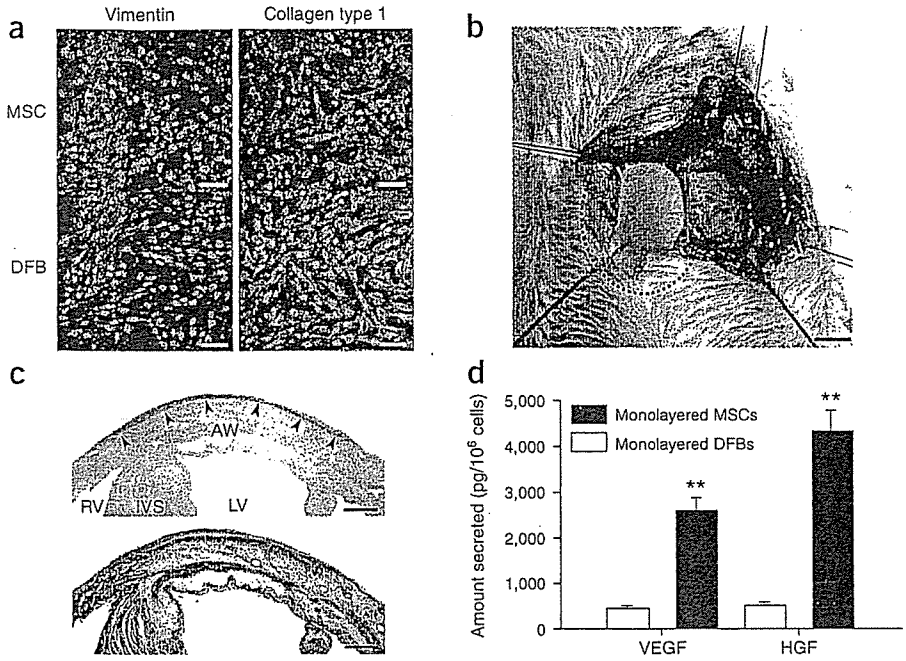

Figure 2 Characteristics of monolayered MSCs. (a) Properties of constituent cells in the monolayered grafts. Compared with DFBs (green), MSCs (green) are positive for vimentin (red) and slightly positive for collagen type 1 (red). (b) Monolayered MSCs (in the dotted circle) transferred to the infarcted heart. (c) Extent of monolayered MSCs 48 h after transplantation (arrows). AW, anterior wall; LV, left ventricle; RV right ventricle; IVS, interventricular septum. (d) Comparison of secretion of growth factors between monolayered MSCs and DFBs. $^{**}P < 0.01$ versus DFBs. Scale bar in a, 20 μm; in b, 5 mm; in c, 100 μm.

before transplantation (**Fig. 2a** and **Supplementary Fig. 1** online), suggesting that the MSC tissue includes a number of undifferentiated MSCs. Taken together, the grown MSC tissue was composed of newly formed blood vessels, undifferentiated MSCs and few cardiomyocytes.

Fluorescence *in situ* hybridization analysis

We performed fluorescence *in situ* hybridization (FISH) to detect X and Y chromosomes after sex-mismatched transplantation of monolayered MSCs. We transplanted GFP-expressing monolayered MSCs derived from male rats to female Sprague-Dawley rats that had suffered an infarct. Four weeks later, newly formed cardiomyocytes that were positive for GFP had only one set of X and Y chromosomes, whereas we detected two X chromosomes exclusively in GFP^- host-derived cells (**Fig. 4h**). We counted the X and Y chromosomes in male and female control rats and in the MSC sheet–transplanted rats (**Supplementary Table 2** online), and we did not detect extra copies of the X or Y chromosome in graft-derived GFP^+ cardiomyocytes. When we compared the frequencies of the occurrence of zero, one, two and more than two X chromosomes in the GFP^+ cardiomyocytes with the frequencies in male control cardiomyocytes, the GFP^+ cardiomyocytes did not show an increased proportion of X chromosomes ($0.25 > P > 0.10$, χ^2 test).

Effects of monolayered MSCs on cardiac function

Heart failure developed 8 weeks after coronary ligation, as indicated by an increase in left ventricle end-diastolic pressure (LVEDP) and attenuation of maximum and minimum rate of change in left ventricular pressure (dP/dt). Autologous transplantation of monolayered MSCs, however, resulted in decreased LVEDP (**Fig. 5a**). Left ventricle maximum and minimum dP/dt were significantly improved in the MSC group (**Fig. 5b,c**). We did not observe these hemodynamic improvements in the DFB group. The MSC group also had significantly lower right ventricular weight and lung weight than the DFB and untreated groups 4 weeks after transplantation (**Supplementary Table 1** online). These results suggest that transplantation of monolayered MSCs has beneficial hemodynamic effects in rats with chronic heart failure.

Echocardiographic analysis showed that transplantation of monolayered MSCs significantly increased diastolic thickness of the infarcted anterior wall (**Fig. 5d**). Left ventricle end-diastolic dimension at 8 weeks was significantly smaller in the MSC group than in the DFB and untreated groups (**Fig. 5e**). Transplantation of the monolayered MSCs significantly increased left ventricle fractional shortening (**Fig. 5f**). Left ventricle wall stress in diastole was markedly lower in the MSC group than in the DFB and untreated groups (**Supplementary Table 3** online). Plasma atrial natriuretic peptide (ANP) in the DFB and untreated groups was markedly elevated 8 weeks after myocardial infarction (**Fig. 5g**). Transplantation of the monolayered MSCs inhibited the increase in plasma ANP.

Survival analysis

The Kaplan-Meier survival curve showed that 4-week survival after coronary ligation did not differ significantly between the untreated and MSC groups before transplantation (**Fig. 5h**). Notably, however, no rats died after transplantation of monolayered MSCs. Therefore, the survival rate after transplantation was markedly higher in the MSC group than in the untreated group (4-week survival after transplantation was 100% for the MSC group versus 71% for the untreated group, log-rank test, $P < 0.05$).

DISCUSSION

There are several advantages to monolayered MSC transplantation. First, the self-propagating property of MSCs *in situ* leads to the formation of a thick stratum on the surface of the scarred myocardium. Second, the multipotency of MSCs and their ability to supply angiogenic cytokines allows neovascularization in the MSC tissue. Third, the reconstruction of thick myocardial tissue reduces left ventricle wall stress and results in improvement of cardiac function after myocardial infarction. Finally, a substantial part of the transplanted tissue is composed of undifferentiated MSCs, and it is tempting to speculate that such cells may act against future progressive left ventricle remodeling.

Cellular cardiomyoplasty using needle injections is emerging as a treatment option for individuals with chronic heart failure, but it may be limited by failure to regenerate cardiac mass. The cell sheet allows for cell-to-cell connections owing to the lack a need for enzymatic digestion[6–10]. Thus, the cell sheet has attracted considerable interest as a tool for tissue engineering[28]. Here, we used adipose tissue–derived MSCs as a cellular source for the cell sheet, which resulted in successful autologous transplantation in heterogenic rats without immunological

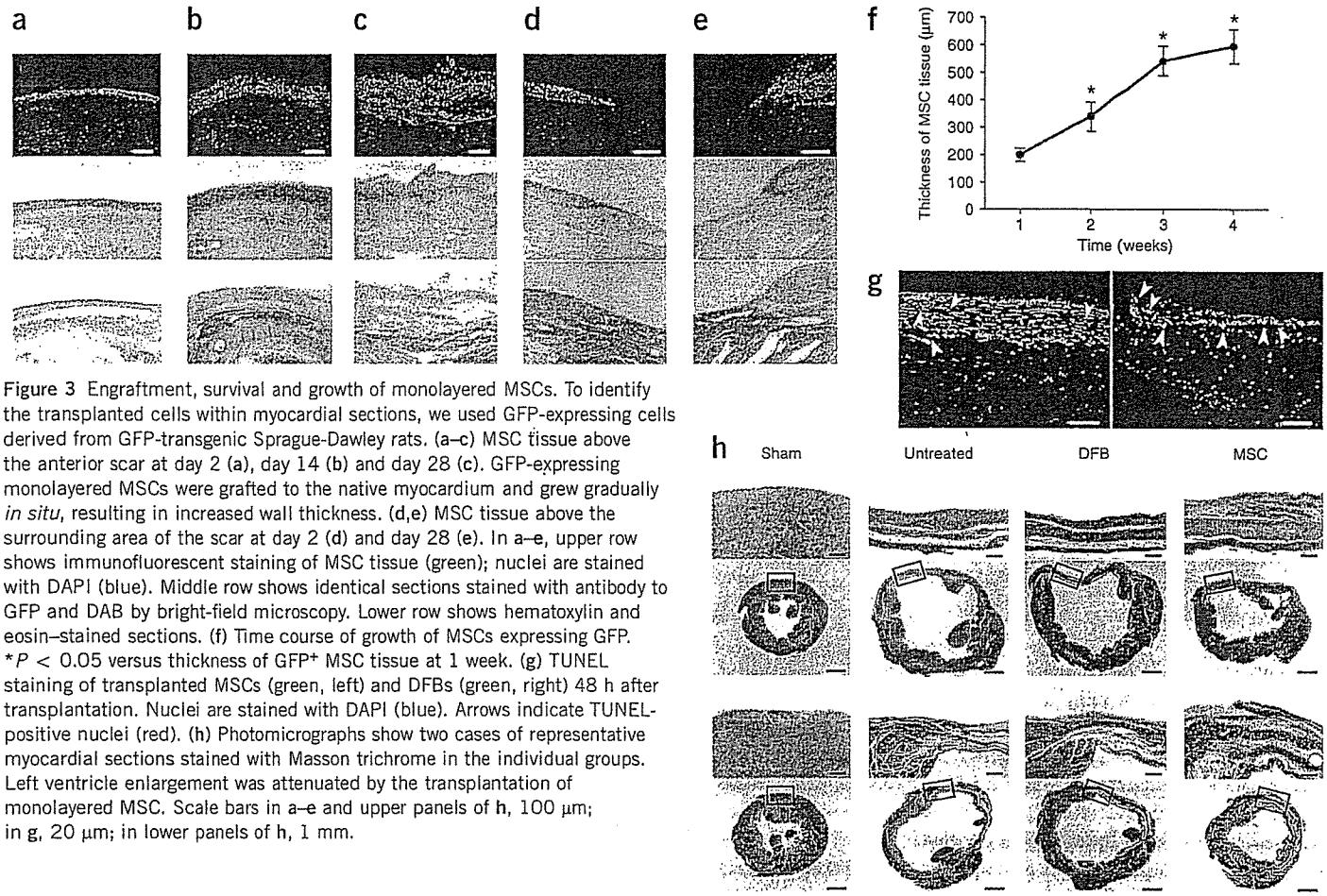

Figure 3 Engraftment, survival and growth of monolayered MSCs. To identify the transplanted cells within myocardial sections, we used GFP-expressing cells derived from GFP-transgenic Sprague-Dawley rats. (a–c) MSC tissue above the anterior scar at day 2 (a), day 14 (b) and day 28 (c). GFP-expressing monolayered MSCs were grafted to the native myocardium and grew gradually *in situ*, resulting in increased wall thickness. (d,e) MSC tissue above the surrounding area of the scar at day 2 (d) and day 28 (e). In a–e, upper row shows immunofluorescent staining of MSC tissue (green); nuclei are stained with DAPI (blue). Middle row shows identical sections stained with antibody to GFP and DAB by bright-field microscopy. Lower row shows hematoxylin and eosin–stained sections. (f) Time course of growth of MSCs expressing GFP. $^*P < 0.05$ versus thickness of GFP$^+$ MSC tissue at 1 week. (g) TUNEL staining of transplanted MSCs (green, left) and DFBs (green, right) 48 h after transplantation. Nuclei are stained with DAPI (blue). Arrows indicate TUNEL-positive nuclei (red). (h) Photomicrographs show two cases of representative myocardial sections stained with Masson trichrome in the individual groups. Left ventricle enlargement was attenuated by the transplantation of monolayered MSC. Scale bars in a–e and upper panels of h, 100 μm; in g, 20 μm; in lower panels of h, 1 mm.

rejection. Using flow cytometry, we did not find any substantial differences between adipose tissue–derived MSCs and bone marrow–derived MSCs, consistent with results from previous studies[22,25]. Adipose-derived MSCs readily attached to and propagated on the temperature-responsive dish. Abdominal subcutaneous adipose tissue is clinically redundant and easily accessible by rapid and minimally invasive surgery such as liposuction. Thus, adipose tissue may serve as a source of stem cells for therapeutic cell sheets.

Here, monolayered MSCs could readily be transferred and grafted to the scarred myocardium without additives or suturing. This may be attributable to cell-to-cell connections as well as extracellular matrix deposits on the basal surface of the monolayered MSCs. Regeneration of myocardial mass is thought to require multilayered constructs of the cell sheet. Unfortunately, however, the lack of a vascular network has limited the formation of a thick construct[10,29]. The transplanted monolayered MSCs thickened gradually, developing into a stratum of up to 600 μm in thickness over the native tissue 4 weeks after transplantation, suggesting that monolayered MSCs have an ability to grow *in situ*. As a result, the transplanted MSC tissue reversed wall thinning of the infarcted myocardium. On the other hand, the fibroblast sheet did not grow *in situ*. It should be noted that the MSC tissue included a large number of newly formed blood vessels. These vessels were composed of graft-derived cells, host-derived cells or both. The MSC sheet secreted a large amount of angiogenic and antiapoptotic cytokines, including VEGF and HGF, as compared with the fibroblast sheet. These results suggest that MSCs induce neovascularization within the sheet not only through their ability to differentiate into vascular cells but also through growth factor–mediated paracrine regulation. Thus, we believe that the angiogenic action of MSCs is important for reconstruction of cardiac mass by the MSC tissue.

Four weeks after transplantation, a small fraction of the engrafted MSCs were positive for cardiac proteins such as cardiac troponin T and desmin, suggesting the presence of cardiomyocytes within the MSC tissue. FISH analysis suggested that the most cardiomyocytes within the MSC tissue were not derived from cell fusion, but we are unable to exclude the possibility that some were. Further studies are necessary to investigate the mechanisms by which MSCs within the MSC tissue regenerate cardiomyocytes. The majority of the MSC tissue was positive for vimentin, a marker for undifferentiated MSCs and fibroblasts. In addition, the majority of MSCs within the graft were negative for collagen type 1 and αSMA, a marker for myofibroblasts. These results suggest that the grown-up MSC tissue is composed of newly formed blood vessels, undifferentiated MSCs and few cardiomyocytes.

We have also shown that transplantation of the monolayered MSCs significantly increased left ventricle maximum dP/dt, decreased LVEDP and inhibited the development of left ventricle enlargement in rats with chronic heart failure secondary to myocardial infarction. These results suggest that transplantation of monolayered MSCs improves cardiac function. But the presence of cardiomyocytes within the MSC tissue seemed to be rare. Thus, this improvement may be explained mainly by growth factor–mediated paracrine effects of the MSC sheet and a decrease in left ventricle wall stress resulting from the thick MSC tissue. Furthermore, no rats treated with the monolayered MSCs died during the study period, although untreated rats died frequently. These results indicate that fatal arrythmogenic problems were not caused by integration of the MSC tissue.

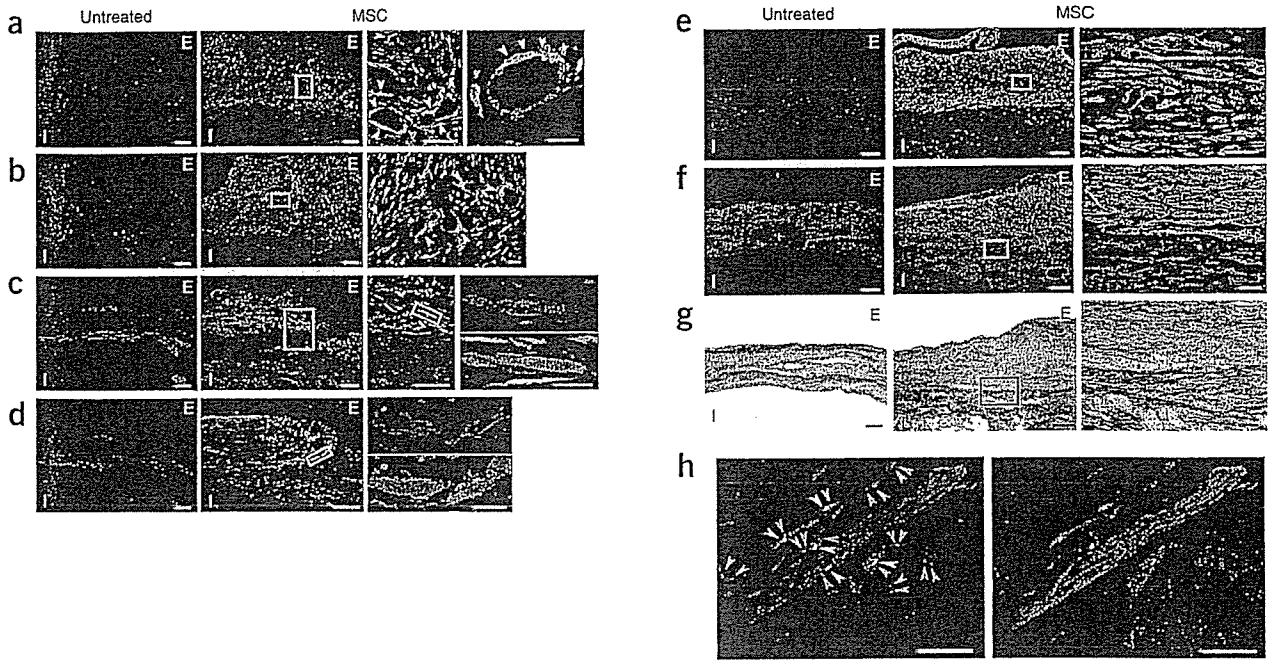

Figure 4 Differentiation of MSCs within the MSC tissue after growth *in situ*. (a,b) GFP-expressing MSCs (green) were identified as a thick stratum at the epicardial side of the myocardium. The MSC tissue contained a number of vascular structures positive for vWF (red, a) and αSMA (red, b). MSCs that did not participate in blood vessel formation were only rarely positive for αSMA, a marker for myofibroblasts. Arrows indicate transplanted MSCs positive for vWF or αSMA. (c,d) Some MSCs within the MSC tissue were positive for cardiac markers cardiac troponin T (red, c) and desmin (red, d). (e) Most of the MSC tissue was positive for vimentin (red). (f) The MSC tissue modestly stained for collagen type 1 (red). (g) Collagen deposition was also detected by picrosirius red staining. (h) FISH analysis. Newly formed cardiomyocytes (desmin, red) that were positive for GFP (green) had only one set of X (purple) and Y chromosomes (white), whereas two X chromosomes were detected exclusively in GFP$^-$ host-derived cells. Nuclei are stained with DAPI (blue, a–f and h). Scale bars in left three panels of a and c and in two left panels of b and d–g, 100 μm; in h and far right panels of a–g, 20 μm. E, epicardial side; I, intimal side.

In summary, adipose tissue–derived monolayered MSCs can be readily engrafted to the scarred myocardium, grow gradually *in situ* and become a thick stratum that includes newly formed vessels, cardiomyocytes and undifferentiated MSCs. The engrafted MSCs reversed wall thinning in the scar area and improved cardiac function and survival in rats with myocardial infarction. Thus, transplantation of monolayered MSCs may be a new therapeutic strategy for cardiac tissue regeneration.

METHODS

Model of heart failure. All protocols were performed in accordance with the guidelines of the Animal Care Ethics Committee of the Japanese National Cardiovascular Center Research Institute. We used male Sprague-Dawley rats (Japan SLC) weighing 187–215 g. A myocardial infarction model was produced by ligation of the left coronary artery, as described previously[30]. Briefly, we anesthetized rats with sodium pentobarbital (30 mg/kg) and ventilated them with a volume-regulated respirator. We exposed hearts by left thoracotomy, and ligated the left coronary artery 2–3 mm from its origin between the pulmonary artery conus and the left atrium with a 6-0 Prolene suture. The sham group underwent thoracotomy and cardiac exposure without coronary ligation. The surviving rats were maintained on standard rat chow.

Study protocol. We randomly placed rats into four groups: rats with chronic heart failure that underwent transplantation of monolayered MSCs (MSC group; $n = 12$), rats with chronic heart failure given monolayered DFBs (DFB group; $n = 12$), rats with chronic heart failure without transplantation (untreated group; $n = 12$) and sham-operated rats without transplantation (sham group; $n = 10$). Four weeks after coronary ligation, the MSC and DFB groups underwent autologous transplantation of each monolayered cell graft onto the anterior wall, including the scar area (**Supplementary Methods** online). The other two groups underwent the same operative procedures without transplantation. We performed hemodynamic studies, echocardiography and histological assessments 4 and 8 weeks after coronary ligation (**Supplementary Methods**). Upon killing at 8 weeks after coronary ligation, only those rats with infarct size >25% of the left ventricle area were included in this study. Therefore, the variation in infarct size between the experimental rats was relatively low (28–41%, average 33.9% ± 1.9%).

Isolation and culture of MSCs from adipose tissue. Immediately after coronary ligation, we acquired subcutaneous adipose tissue (1.1 ± 0.1 g) from the right inguinal region of each rat. We minced adipose tissue with scissors and digested it with 10 ml of type 1 collagenase solution (0.1 mg/ml, Worthington Biochemical) for 1 h in a 37 °C water bath shaker. After filtration with mesh filter (Costar 3480, Corning) and centrifugation at 780*g* for 8 min, we suspended isolated cells in α-MEM supplemented with 10% FCS and antibiotics, plated them onto a 100-mm dish and incubated them at 37 °C with 5% CO_2. A small number of spindle-shaped cells were apparent in visible symmetric colonies by days 5–7.

Preparation of temperature-responsive dishes. Specific procedures for preparation of square-designed PIPAAm-grafted dishes have been previously described[9]. Briefly, we spread IPAAm monomer (Kohjin) in 2-propanol solution onto 60-mm polystyrene culture dishes (Corning). We then subjected the dishes to irradiation (0.25-MGy electron beam dose) using an Area Beam Electron Processing system (Nisshin High-Voltage) to immobilize IPAAm on the dish surface; we then rinsed dishes with cold distilled water and dried them in nitrogen gas. In the second step, we masked the PIPAAm-grafted surface with a square glass coverslip (24 × 24 mm, Matsunami Glass). We spread acrylamide (AAm) monomer solution in 2-propanol onto the masked dish surface. We then irradiated the dish surface with an electron beam and washed it. As a result, the central square area of each dish was PIPAAm grafted (temperature responsive), and the surrounding border was poly-AAm grafted (non–cell adhesive). This PIPAAm-grafted surface is hydrophobic under culture

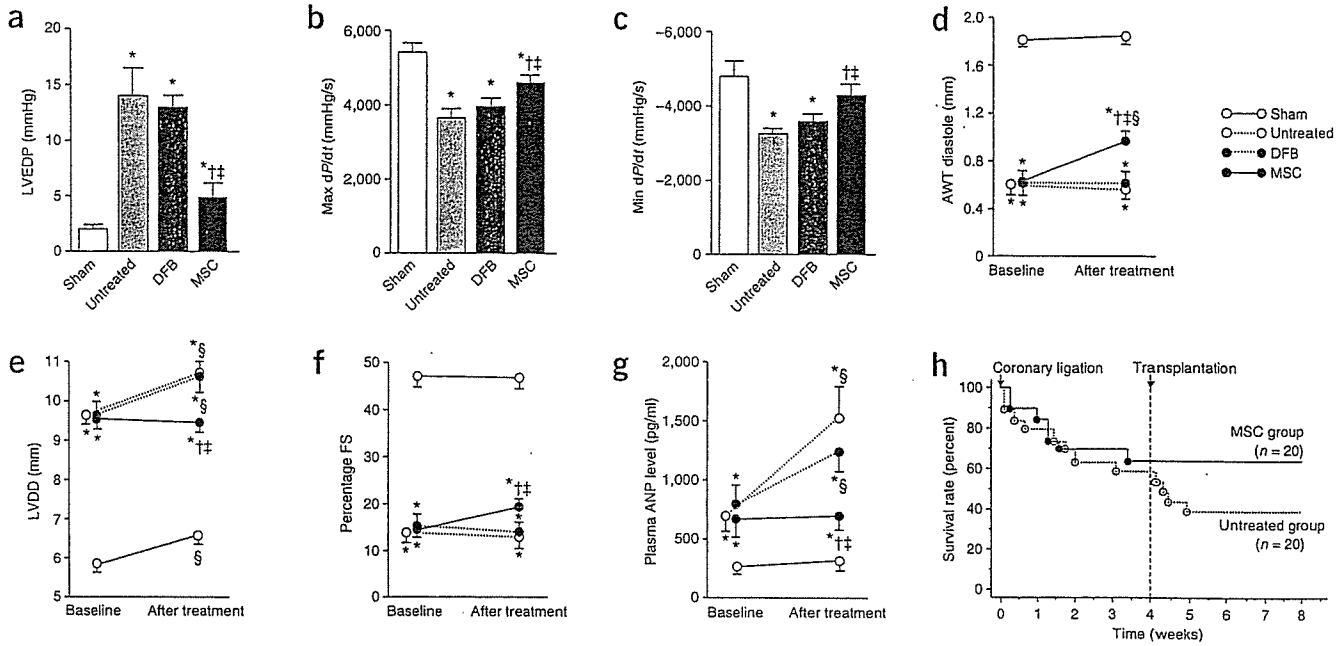

Figure 5 Cardiac structure and function after transplantation of monolayered MSCs. (a–c) Hemodynamic parameters obtained by catheterization. LVEDP, left ventricle end-diastolic pressure. (d–f) Echocardiographic findings. AWT, anterior wall thickness; LVDD, left ventricle end-diastolic dimension; FS, fractional shortening. (g) Plasma atrial natriuretic peptide (ANP) level. Baseline represents measurements 4 weeks after coronary ligation; 'after treatment' represents measurements taken 4 weeks after transplantation (8 weeks after coronary ligation). Data are mean ± s.e.m. $^{*}P < 0.05$ versus sham group; $^{\dagger}P < 0.05$ versus untreated group; $^{\ddagger}P < 0.05$ versus DFB group; $^{\S}P < 0.05$ versus baseline. (h) Survival of rats with chronic heart failure with or without monolayered MSC transplantation. The Kaplan-Meier survival curve demonstrates an 8-week survival rate of 65% for the MSC group versus 45% for the untreated group. Survival rate after transplantation was significantly higher in the MSC group than in the untreated group (100% versus 71% 4-week survival rate after transplantation, log-rank test, $P < 0.05$).

conditions at 37 °C and becomes reversibly hydrophilic below 32 °C. Therefore, cultured cells that adhere to the dish surface spontaneously detach from the grafted surface without enzymatic digestion.

Preparation of monolayered cell grafts. We suspended MSCs at the third or fourth passage from adipose tissue or DFBs at the second passage by trypsinization, and plated the cell suspension containing 3 ml of complete medium onto a 60-mm temperature-responsive dish at 5×10^5 cells per dish (MSCs) or 8×10^5 cells per dish (DFBs) and cultured cells at 37 °C. After 3 d of culture, confluently cultured MSCs or DFBs on the temperature-responsive dishes were incubated at 20 °C. By 40 min, both MSCs and DFBs detached spontaneously and floated up into the medium as monolayered cell grafts. Immediately after detachment, we gently aspirated the monolayered cell grafts using a 1,000 µl pipette tip and transferred them onto an elastic plastic sheet.

Statistical analysis. Numerical values are expressed as mean ± s.e.m. There are four groups of continuous variables in this study. Therefore, for multiple comparisons of more than two groups, we performed one-way analysis of variance (ANOVA). If the ANOVA was significant, we used the Newman-Keul procedure as a *post hoc* test. For repeated measurement such as echocardiographic parameters, we performed two-way repeated ANOVA with the Newman-Keul test. Comparisons of parameters between two groups were made by unpaired Student *t*-test. A value of $P < 0.05$ was considered significant.

Note: Supplementary information is available on the Nature Medicine website.

ACKNOWLEDGMENTS

We thank J.I. Hoffman for his statistical advice. We thank T. Iwase, T. Ito, S. Murakami, N. Sakata and Y. Isono for their technical support. We thank Y. Tsuboi and H. Sonoda for their assistance with microscopic analysis of monolayered cell grafts. We also thank Y. Sawa for his suggestions on this study. This work was supported by research grants for Cardiovascular Disease (16C-6) and Human Genome Tissue Engineering 005 and 009 from the Japanese Ministry of Health, Labor and Welfare, and the Program for Promotion of Fundamental Studies in Health Science of the Japanese National Institute of Biomedical Innovation.

COMPETING INTERESTS STATEMENT

The authors declare competing financial interests (see the *Nature Medicine* website for details).

Published online at http://www.nature.com/naturemedicine/
Reprints and permissions information is available online at http://npg.nature.com/reprintsandpermissions/

1. Liu, J. *et al.* Autologous stem cell transplantation for myocardial repair. *Am. J. Physiol. Heart Circ. Physiol.* 287, H501–H511 (2004).
2. Reinlib, L. & Field, L. Cell transplantation as future therapy for cardiovascular disease?: A workshop of the National Heart, Lung, and Blood Institute. *Circulation* 101, E182–E187 (2000).
3. Schuster, M.D. *et al.* Myocardial neovascularization by bone marrow angioblasts results in cardiomyocyte regeneration. *Am. J. Physiol. Heart Circ. Physiol.* 287, H525–H532 (2004).
4. Kocher, A.A. *et al.* Neovascularization of ischemic myocardium by human bone-marrow-derived angioblasts prevents cardiomyocyte apoptosis, reduces remodeling and improves cardiac function. *Nat. Med.* 7, 430–436 (2001).
5. Bel, A. *et al.* Transplantation of autologous fresh bone marrow into infarcted myocardium: a word of caution. *Circulation* 108, II247–II252 (2003).
6. Yamada, N. *et al.* Thermo-responsive polymeric surface: control of attachment and detachment of cultured cells. *Makromol. Chem. Rapid Commun.* 11, 571–576 (1990).
7. Okano, T., Yamada, H., Sakai, H. & Sakurai, Y. A novel recovery system for cultured cells using plasma-treated polystyrene dishes grafted with poly (N-isopropylacrylamide). *J. Biomed. Mater. Res.* 27, 1243–1251 (1993).
8. Shimizu, T. *et al.* Fabrication of pulsatile cardiac tissue grafts using a novel 3-dimensional cell sheet manipulation technique and temperature-responsive cell culture surfaces. *Circ. Res.* 90, e40–e48 (2002).
9. Hirose, M., Kwon, O.H., Yamato, M., Kikuchi, A. & Okano, T. Creation of designed shape cell sheets that are noninvasively harvested and moved onto another surface. *Biomacromolecules* 1, 377–381 (2000).
10. Kushida, A. *et al.* Decrease in culture temperature releases monolayer endothelial cell sheets together with deposited fibronectin matrix from temperature-responsive culture surfaces. *J. Biomed. Mater. Res.* 45, 355–362 (1999).
11. Herreros, J. *et al.* Autologous intramyocardial injection of cultured skeletal muscle-derived stem cells in patients with non-acute myocardial infarction. *Eur. Heart J.* 24, 2012–2020 (2003).

12. Skobel, E. *et al.* Transplantation of fetal cardiomyocytes into infarcted rat hearts results in long-term functional improvement. *Tissue Eng.* **10**, 849–864 (2004).
13. Hodgson, D.M. *et al.* Stable benefit of embryonic stem cell therapy in myocardial infarction. *Am. J. Physiol. Heart Circ. Physiol.* **287**, H471–H479 (2004).
14. Makino, S. *et al.* Cardiomyocytes can be generated from marrow stromal cells in vitro. *J. Clin. Invest.* **103**, 697–705 (1999).
15. Pittenger, M.F. *et al.* Multilineage potential of adult human mesenchymal stem cells. *Science* **284**, 143–147 (1999).
16. Reyes, M. *et al.* Origin of endothelial progenitors in human postnatal bone marrow. *J. Clin. Invest.* **109**, 337–346 (2002).
17. Toma, C., Pittenger, M.F., Cahill, K.S., Byrne, B.J. & Kessler, P.D. Human mesenchymal stem cells differentiate to a cardiomyocyte phenotype in the adult murine heart. *Circulation* **105**, 93–98 (2002).
18. Wang, J.S. *et al.* Marrow stromal cells for cellular cardiomyoplasty: feasibility and potential clinical advantages. *J. Thorac. Cardiovasc. Surg.* **120**, 999–1005 (2000).
19. Jiang, Y. *et al.* Pluripotency of mesenchymal stem cells derived from adult marrow. *Nature* **418**, 41–49 (2002).
20. Nagaya, N. *et al.* Transplantation of mesenchymal stem cells improves cardiac function in a rat model of dilated cardiomyopathy. *Circulation* **112**, 1128–1135 (2005).
21. Rangappa, S., Fen, C., Lee, E.H., Bongso, A. & Wei, E.S. Transformation of adult mesenchymal stem cells isolated from the fatty tissue into cardiomyocytes. *Ann. Thorac. Surg.* **75**, 775–779 (2003).
22. Zuk, P.A. *et al.* Human adipose tissue is a source of multipotent stem cells. *Mol. Biol. Cell* **13**, 4279–4295 (2002).
23. Gaustad, K.G., Boquest, A.C., Anderson, B.E., Gerdes, A.M. & Collas, P. Differentiation of human adipose tissue stem cells using extracts of rat cardiomyocytes. *Biochem. Biophys. Res. Commun.* **314**, 420–427 (2004).
24. Planat-Benard, V. *et al.* Plasticity of human adipose lineage cells toward endothelial cells: physiological and therapeutic perspectives. *Circulation* **109**, 656–663 (2004).
25. Lee, R.H. *et al.* Characterization and expression analysis of mesenchymal stem cells from human bone marrow and adipose tissue. *Cell. Physiol. Biochem.* **14**, 311–324 (2004).
26. Li, J., Takaishi, K., Cook, W., McCorkle, S.K. & Unger, R.H. Insig-1 "brakes" lipogenesis in adipocytes and inhibits differentiation of preadipocytes. *Proc. Natl. Acad. Sci. USA* **100**, 9476–9481 (2003).
27. Vande Berg, J.S., Rudolph, R. & Woodward, M. Comparative growth dynamics and morphology between cultured myofibroblasts from granulating wounds and dermal fibroblasts. *Am. J. Pathol.* **114**, 187–200 (1984).
28. Nishida, K. *et al.* Corneal reconstruction with tissue-engineered cell sheets composed of autologous oral mucosal epithelium. *N. Engl. J. Med.* **351**, 1187–1196 (2004).
29. Shimizu, T., Yamato, M., Kikuchi, A. & Okano, T. Cell sheet engineering for myocardial tissue reconstruction. *Biomaterials* **24**, 2309–2316 (2003).
30. Nishikimi, T., Uchino, K. & Frohlich, E.D. Effects of α1-adrenergic blockade on intrarenal hemodynamics in heart failure rats. *Am. J. Physiol. Regul. Integr. Comp. Physiol.* **262**, R198–R203 (1998).

Available online at www.sciencedirect.com
ScienceDirect
ELSEVIER
Biochemical and Biophysical Research Communications 349 (2006) 1242–1249
BBRC
www.elsevier.com/locate/ybbrc

Beraprost sodium enhances neovascularization in ischemic myocardium by mobilizing bone marrow cells in rats

Yoshinori Miyahara [a], Shunsuke Ohnishi [a], Hiroaki Obata [a], Kozo Ishino [b], Shunji Sano [b], Hidezo Mori [c], Kenji Kangawa [d], Soichiro Kitamura [e], Noritoshi Nagaya [a,*]

[a] *Department of Regenerative Medicine and Tissue Engineering, National Cardiovascular Center Research Institute, Osaka, Japan*
[b] *Department of Cardiovascular Surgery, Okayama University Graduate School of Medicine, Dentistry and Pharmaceutical Sciences, Okayama, Japan*
[c] *Department of Cardiac Physiology, National Cardiovascular Center Research Institute, Osaka, Japan*
[d] *Department of Biochemistry, National Cardiovascular Center Research Institute, Osaka, Japan*
[e] *Department of Cardiovascular Surgery, National Cardiovascular Center, Osaka, Japan*

Received 13 August 2006
Available online 7 September 2006

Abstract

Beraprost sodium, an orally active prostacyclin analogue, has vasoprotective effects such as vasodilation and antiplatelet activities. We investigated the therapeutic potential of beraprost for myocardial ischemia. Immediately after coronary ligation of Sprague–Dawley rats, beraprost (200 μg/kg/day) or saline was subcutaneously administered for 28 days. Four weeks after coronary ligation, administration of beraprost increased capillary density in ischemic myocardium, decreased infarct size, and improved cardiac function in rats with myocardial infarction. Beraprost markedly increased the number of CD34-positive cells and c-kit-positive cells in plasma. Also, four weeks after coronary ligation of chimeric rats with GFP-expressing bone marrow, bone marrow-derived cells were incorporated into the infarcted region and its border zone. Treatment with beraprost increased the number of GFP/von Willebrand factor-double-positive cells in the ischemic myocardium. These results suggest that beraprost has beneficial effects on ischemic myocardium partly by its ability to enhance neovascularization in ischemic myocardium by mobilizing bone marrow cells.

Keywords: Prostacyclin analogue; Myocardial infarction; Neovascularization; Bone marrow mobilization

Interruption of myocardial blood flow leads to rapid death of cardiomyocytes and vascular structures, resulting in the development of heart failure [1]. Stem or progenitor cells are mobilized from bone marrow into the peripheral blood in response to tissue ischemia, migrate to sites of injured tissues, and differentiate into endothelial cells and cardiomyocytes [2–4]. However, the compensatory mechanisms are insufficient to heal infarcted myocardium. Earlier studies have shown that bone marrow cells artificially mobilized by cytokines repair the infarcted heart and improve cardiac function after acute myocardial infarction [5,6]. Therefore, enhancement of bone marrow cell mobilization leading to neovascularization following revascularization would be beneficial for the treatment of acute myocardial infarction.

Beraprost sodium (BPS) is a chemically stable prostacyclin analogue owing to its cyclo-pentabenzofuranyl structure [7]. It has been well established that BPS has vasoprotective effects such as vasodilation and antiplatelet activities [8–11]. Thus, BPS has been used in the treatment of peripheral arterial disease [12,13] and pulmonary arterial hypertension [14,15]. Although a limited number of studies suggest therapeutic potential of prostacyclin for the treatment of myocardial ischemia [16–18], the underlying mechanisms still remain unclear. In addition, little information is available regarding the therapeutic potential of prostacyclin analogues such as BPS for myocardial ischemia. A recent study has shown that BPS activates endothelial

* Corresponding author. Fax: +81 6 6833 9865.
E-mail address: nnagaya@ri.ncvc.go.jp (N. Nagaya).

0006-291X/$ - see front matter © 2006 Elsevier Inc. All rights reserved.
doi:10.1016/j.bbrc.2006.08.178

nitric oxide synthase (eNOS) through the c-AMP/protein kinase A pathway [19]. Activation of eNOS is known to contribute to bone marrow cell mobilization, leading to neovascularization [20]. These results raise the possibility that BPS may have beneficial effects on the ischemic myocardium through enhancement of bone marrow cell mobilization.

Thus, the purposes of this study were: (1) to examine the effect of BPS on mobilization and recruitment of bone marrow cells after acute myocardial infarction, (2) to investigate whether BPS induces neovascularization in the ischemic myocardium, and (3) to investigate whether treatment with BPS improves cardiac function in rats with myocardial infarction.

Methods

Model of myocardial infarction. We used male Sprague–Dawley rats (Japan SLC Inc., Hamamatsu, Japan) weighing 185–215 g. Myocardial infarction was produced by left coronary ligation, as described previously [21]. Briefly, after rats were anesthetized with sodium pentobarbital (30 mg/kg), they were artificially ventilated with a volume-regulated respirator. The heart was exposed via a left thoracotomy incision. Then, the left coronary artery was ligated 2–3 mm from its origin between the pulmonary artery conus and the left atrium with a 6-0 Prolene suture. Finally, the heart was restored to its normal position, and the chest was closed. Experimental protocols were performed in accordance with the "Guidelines of the Animal Care Ethics Committee of the National Cardiovascular Center Research Institute", which complies NIH Guidelines.

Administration of BPS. Immediately after coronary ligation, BPS (200 μg/kg/day, Astellas Pharma Inc., Tokyo, Japan) was subcutaneously administered to surviving rats using an osmotic mini-pump for 4 weeks (BPS group, $n = 12$). As a control, saline was similarly administered to rats receiving coronary ligation (Control group, $n = 12$).

Echocardiographic studies. Echocardiographic studies were performed 4 weeks after coronary ligation. M-mode tracings were obtained at the level of the papillary muscles using an echocardiographic system equipped with a 7.5-MHz phased-array transducer (HP SONOS 5500; Hewlett Packard Co., Andover, MA). Anterior and posterior end-diastolic and end-systolic wall thickness, LV end-diastolic and end-systolic dimensions, and LV fractional shortening were measured by the American Society for Echocardiography leading-edge method in three consecutive cardiac cycles. LV meridional wall stress was estimated as $0.344 \times \text{LV pressure} \times \{\text{LV dimension}/(1 + \text{PWT/LV dimension})\}$, where PWT is posterior wall thickness [22].

Hemodynamic studies. Hemodynamic studies were performed 4 weeks after coronary ligation, following echocardiography. After anesthesia with pentobarbital sodium, a 1.5F micromanometer-tipped catheter (Millar Instruments Inc., Houston, TX) was advanced into the LV through the right common carotid artery. Hemodynamic variables were measured with a pressure transducer connected to a polygraph. After completion of these measurements, the left and right ventricles and the lungs were excised and weighed. Infarct size was determined as a percentage of the entire LV area ($n = 5$ in each group), as reported previously [23]. Briefly, incisions were made in the posterior LV so that the tissue could be pressed flat. The circumference of the entire flat LV and of the visualized infarcted area, as judged from both the epicardial and endocardial sides, was outlined on a clear plastic sheet. The difference in weight between the two marked areas on the sheet was used to determine infarct size and was expressed as a percentage of LV surface area.

Measurement of plasma ANP level. Blood samples were obtained 4 weeks after coronary ligation. Plasma atrial natriuretic peptide (ANP), a marker for heart failure, was measured by enzyme immunoassay (Peninsula Laboratories Inc., San Carlos, CA).

Mononuclear cell mobilization and FACS analysis. To investigate whether administration of BPS mobilizes bone marrow cells, an additional 12 rats were randomized to receive BPS (200 μg/kg/day, BPS group, $n = 6$) or saline (Control group, $n = 6$). On the third day of BPS or saline treatment, 4 ml of blood was drawn from the inferior vena cava of each rat. Peripheral blood was obtained at the end of infusion. After mononuclear cells were counted, they were incubated for 30 min at 4 °C with fluorescein isothiocyanate (FITC)-conjugated mouse monoclonal antibodies against rat CD34 (clone ICO-115, Santa Cruz) and CD45 (clone OX-1), and FITC-conjugated rabbit anti-rat c-Kit polyclonal antibody (clone C-19, Santa Cruz). Immunofluorescence-labeled cells were analyzed by quantitative flow cytometry with a FACSCalibur flow cytometer (BD Biosciences, Mountain View, CA). Isotype-identical antibodies served as controls.

RT-PCR assay. To investigate whether bone marrow cells express the prostacyclin receptor (IP receptor), we analyzed expression of its mRNA by reverse transcription-polymerase chain reaction (RT-PCR). In brief, total RNA of bone marrow cells was extracted with guanidine isothiocyanate (RNeasy Mini Kit, Qiagen). Then, reverse-transcribed single-stranded cDNA was subjected to PCR (PCR Amplification Kit, Takara) using primer sets for the IP receptor (Hokkaido System Science Co., Ltd., Sapporo, Japan, forward, 5′-GGCACGAGAGGATGAAGTTTACC-3′; reverse, 5′-GTCAGAGGCACAGCAGTCAATGG-3′) and G3PDH (Clonetech Laboratories Inc., Mountain View, CA, forward, 5′-TG AAGGTCGGTGTCAACGGATTTGGC-3′; reverse, 5′-CATGTAGG CCATGAGGTCCACCAC-3′).

Creation of bone marrow-chimeric rats. To assess recruitment of bone marrow cells after BPS administration, bone marrow transplantation was performed by using male normal Sprague–Dawley rats as recipients and male Green fluorescent protein (GFP)-transgenic rats (SD-Tg [Act-EGFP] CZ-004Osb, Japan SLC Inc.) as donors, using a previously described method [24]. Briefly, bone marrow was harvested by flushing the cavity of femurs and tibias from GFP-transgenic rats with phosphate-buffered saline. Then, 3×10^7 GFP-positive bone marrow cells were individually administered to 12 lethally irradiated (900c Gray) rats via the tail vein. Four weeks after transplantation, flowcytometric analysis determined that 90% of peripheral blood mononuclear cells from both donors and 8 of 12 chimeric rats were GFP-positive, suggesting the establishment of stable chimerism. These chimeric rats were subjected to left coronary ligation, followed by administration of BPS (200 μg/kg/day, BPS group, $n = 4$) or saline (Control group, $n = 4$) using an osmotic mini-pump for 4 weeks.

Histological examination. To detect fibrosis in the cardiac muscle, the LV myocardium ($n = 5$, each group) was fixed in 10% formalin, cut transversely in three sections, embedded in paraffin, and stained with Masson's trichrome. To detect capillary endothelial cells in the peri-infarct area, we performed DAB staining (LSAB2 System HRP, Dako Cytomation Co., Denmark) using rabbit polyclonal anti-von Willebrand factor (vWF) antibody (Dako). A total of 10 different fields from three different sections were randomly selected, and the number of capillaries was counted in the peri-infarct area using a light microscope at 200× magnification. Capillary density was expressed as the mean number of capillaries per square millimeter. Also, 4 weeks after coronary ligation in bone marrow-chimeric rats ($n = 4$ in each group), the LV myocardium was excised, embedded in OCT compound, snap-frozen in liquid nitrogen, and cut transversely into 6-μm-thick sections from base to apex. Immunofluorescent staining was performed using rabbit polyclonal anti-vWF antibody (Dako), mouse monoclonal anti-cardiac troponin T antibody (Neomarkers, Fremont, CA), and rabbit polyclonal Alexa 488-conjugated anti-GFP antibody (Molecular Probes Inc., Eugene, OR). The nuclei were counterstained with 4′,6′-diamidino-2-phenylindole (DAPI). We measured the number of GFP/vWF-double-positive cells incorporated into vascular structures in 10 randomly selected fields in the peri-infarct area per section in a blinded fashion using a fluorescence microscope.

Statistical analysis. Numerical values are expressed as means ± SEM. Comparisons of parameters between two groups were made by unpaired Student's t test. A value of $p < 0.05$ was considered significant.

Results

Cardiac structure

Body weight at 4 weeks after coronary ligation was significantly greater in the BPS group than in the Control group (Table 1). Right ventricular weight and lung weight in the BPS group were significantly smaller than those in the Control group, although LV weight did not differ between the two groups. Moderate to large infarcts were observed in the Control group (Fig. 1A). However, administration of BPS significantly decreased infarct size in rats with myocardial infarction (Fig. 1A and B). BPS significantly decreased LV end-diastolic dimension (LVDD) (Fig. 1C).

Table 1
Physiological profiles of experimental groups

	Control	BPS
Number	12	12
Body weight (g)		
Baseline	198 ± 3	204 ± 3
After treatment	319 ± 6	352 ± 9*
LV wt/body wt (g/kg)	2.28 ± 0.04	2.27 ± 0.04
RV wt/body wt (g/kg)	0.99 ± 0.05	0.61 ± 0.02**
Lung wt/body wt (g/kg)	6.55 ± 0.62	3.88 ± 0.1**
Plasma AND level (pg/ml)	798 ± 99	498 ± 57*

Control, infarct rats without treatment; BPS, infarct rats treated with BPS administration; AND, atrial natriuretic protein. Data are expressed as means ± SEM. $^{*}p < 0.05$, $^{**}p < 0.01$ vs. Control group.

Cardiac function

Neither heart rate nor mean arterial pressure differed between the BPS and Control groups (Table 2). LV fractional shortening and LV maximum dP/dt in the BPS group were significantly greater than those in the Control group (Fig. 2A and B). LV end-diastolic pressure (LVEDP) in the BPS group was significantly lower than that in the Control group (Fig. 2C). LV minimum dP/dt was also improved by BPS (Fig. 2D). Treatment with BPS attenuated the increase in plasma ANP level after myocardial infarction (Table 1). BPS significantly increased anterior wall thickening, although it did not significantly alter posterior wall thickening (Table 2). Thickness of the anterior and posterior walls tended to be greater in the BPS group, but these changes did not reach statistical significance. LV diastolic wall stress in the BPS group was significantly lower than that in the Control group.

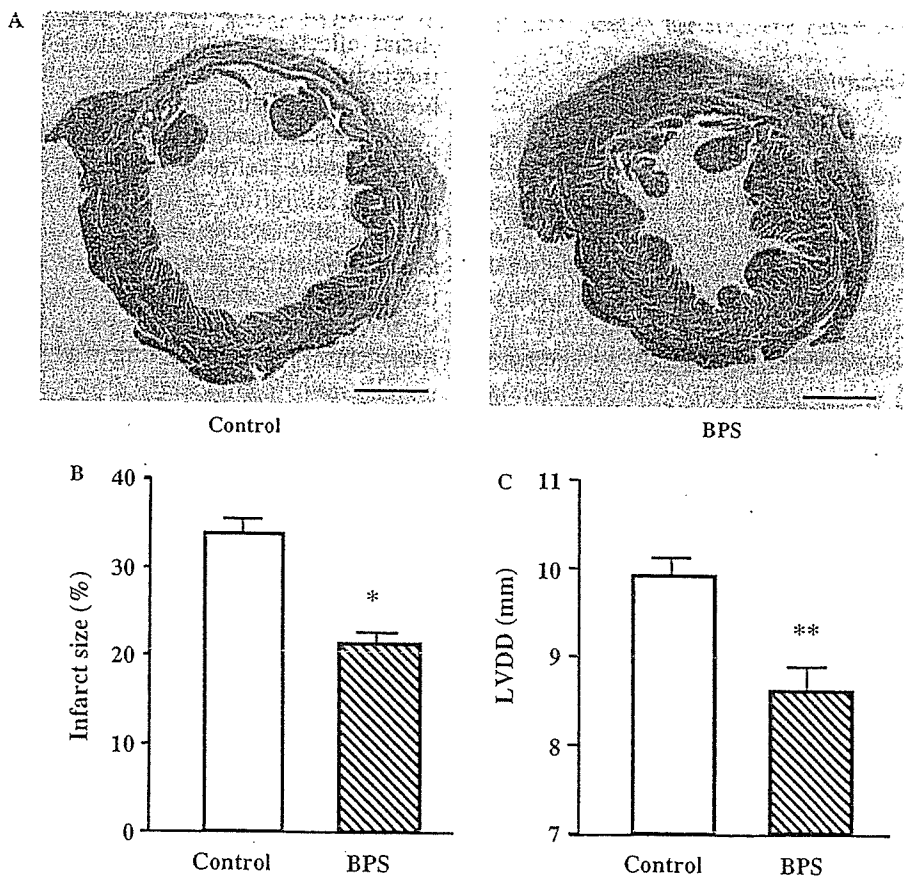

Fig. 1. (A) Representative examples of Masson's trichrome staining of transverse sections of LV myocardium 4 weeks after coronary ligation. Scale bars = 2 mm. (B,C) Quantitative analysis of infarct size and LV end-diastolic dimension (LVDD). Infarcted area and LVDD in the BPS group were significantly smaller than those in the Control group. Data are expressed as means ± SEM. $^{*}p < 0.05$, $^{**}p < 0.01$ vs. Control group.

Table 2
Echocardiographic and hemodynamic data

	Control	BPS
AWT diastole (mm)	0.62 ± 0.04	0.74 ± 0.05
AW thickening (%)	17 ± 3	34 ± 6*
PWT diastole (mm)	1.55 ± 0.07	1.70 ± 0.04
PW thickening (%)	43 ± 4	49 ± 3
Heart rate (bpm)	458 ± 7	471 ± 10
Mean arterial pressure (mmHg)	103 ± 5	115 ± 4
LV systolic pressure (mmHg)	113 ± 4	127 ± 5*
LV diastolic wall stress (kdyne/cm^2)	24 ± 4	5 ± 1**
LV systolic wall stress (kdyne/cm^2)	267 ± 18	225 ± 14

AWT, anterior wall thickness; AW, anterior wall; PWT, posterior wall thickness; PW, posterior wall. Data are expressed as means ± SEM. *$p < 0.05$, **$p < 0.01$ vs. Control group.

Mobilization of bone marrow cells

RT-PCR demonstrated that IP receptor mRNA was expressed in bone marrow cells (Fig. 3A), indicating a direct effect of BPS on these cells. Three-day administration of BPS significantly increased the number of peripheral blood mononuclear cells compared to saline administration (Fig. 3B). Administration of BPS markedly increased the number of circulating progenitor cells such as CD34-positive cells and c-kit-positive cells (Fig. 3C and D). BPS also increased the number of CD45-positive hematopoietic lineage cells (Fig. 3E).

BPS-induced neovascularization

Chimeric rats with GFP-expressing bone marrow were used to assess recruitment of bone marrow cells. Four weeks after coronary ligation, bone marrow-derived GFP-positive cells were incorporated predominantly into the infarcted region and its border zone (Fig. 4A), while these cells were rarely detected in the noninfarcted myocardium. Some of the GFP-positive cells stained for vWF and formed vascular structures. Semi-quantitative analysis demonstrated that the number of GFP-positive cells in the myocardium was significantly greater in the BPS group than in the Control group (Fig. 4B). The number of GFP-vWF double-positive cells (bone marrow-derived endothelial cells) in the ischemic myocardium was significantly greater in the BPS group than in the Control group (Fig. 4C). In addition, a small number of GFP-troponin T-double-positive cells were observed in the BPS group (Fig. 4D).

Capillary density

In the peri-infarct area, clustering of relatively small vessels was seen in BPS-treated hearts, which is indicative of recent endothelial regeneration (Fig. 5A). Semi-quantitative analysis also demonstrated that administration of BPS significantly increased the capillary density in the peri-infarct area compared to the Control group (Fig. 5B).

Discussion

In the present study, we demonstrated that treatment with BPS (1) decreased infarct size and improved cardiac structure and function in rats with acute myocardial infarction, (2) increased the number of circulating progenitor cells such as CD34-positive cells and c-kit-positive cells in rats, and (3) increased the number of bone marrow-derived endothelial cells and the capillary density in the ischemic myocardium. These results suggest that BPS may have beneficial effects on ischemic myocardium at least in part through enhancement of neovascularization by mobilizing bone marrow cells.

Earlier studies have reported that prostacyclin has cardioprotective effects in ischemia–reperfusion injury through inhibition of neutrophil activation and migration [25,26]. BPS is also reported to inhibit chemotaxis and superoxide anion production of neutrophils which contribute to tissue damage by releasing tissue destructive lysosomal enzymes [27]. Infusion of BPS has been shown to reduce infarct size in the dog heart with left coronary occlusion by reducing myocardial oxygen demand and by inhibition of the migration of neutrophils [28]. However, these

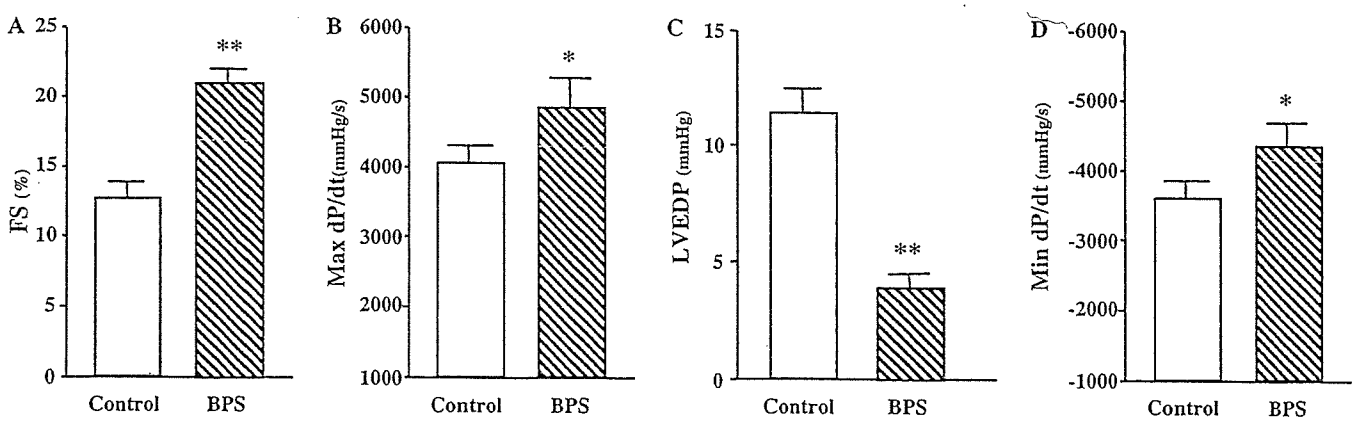

Fig. 2. Cardioprotective effects of BPS on echocardiographic and hemodynamic parameters. FS, fractional shortening; LVEDP, LV end-diastolic pressure; Max and Min dP/dt, maximum and minimum dP/dt. Data are expressed as means ± SEM. *$p < 0.05$, **$p < 0.01$ vs. Control group.

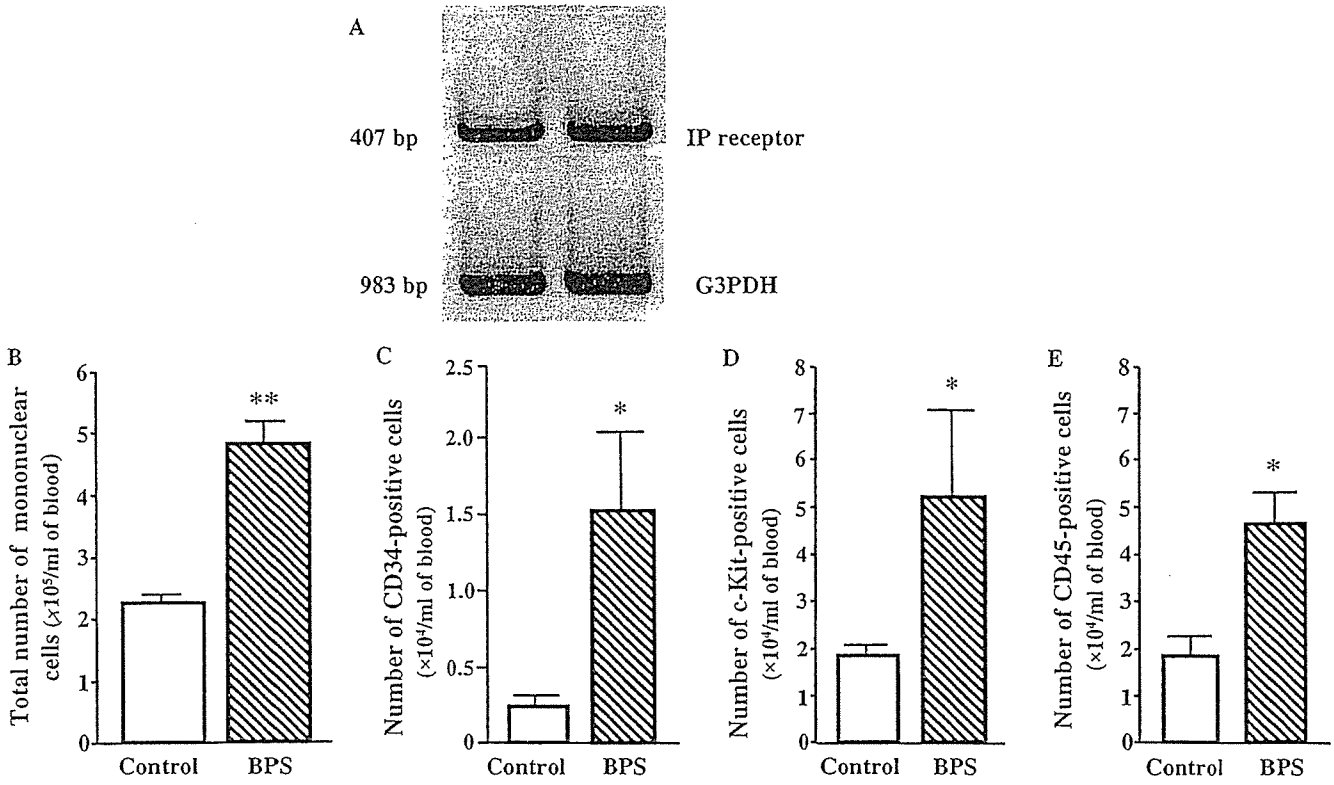

Fig. 3. BPS-induced mobilization of bone marrow cells. (A) Expression of prostacyclin receptor (IP receptor) on bone marrow cells. (B–E) Quantification of BPS-induced MNC mobilization by FACS analysis. Administration of BPS markedly increased the number of circulating progenitor cells such as CD34-positive cells and c-kit-positive cells. BPS also increased the number of CD45-positive hematopoietic lineage cells. Data are expressed as means ± SEM. $^{*}p < 0.05$, $^{**}p < 0.01$ vs. Control group.

biological activities of BPS appear to be insufficient to explain the decrease in infarct size as well as suppression of LV remodeling.

Recent studies have shown that mobilization of bone marrow cells by cytokines promotes myocardial repair and regeneration after acute myocardial infarction [5,6]. In the present study, three-day administration of BPS markedly increased the number of circulating progenitor cells such as CD34-positive cells and c-kit-positive cells in rats. In addition, treatment with BPS enhanced recruitment of bone marrow cells to the ischemic myocardium and increased capillary density in the peri-infarct area. Earlier studies have shown that CD34-positive cells have angiogenic potential to treat ischemic heart [29–31]. Also, another stem cell fraction, c-kit-positive cells have ability to repair ischemic myocardium by differentiating into vascular endothelial cells [32,33]. These findings suggest that administered BPS induces neovascularization partly via enhancement of bone marrow cell mobilization. RT-PCR demonstrated that IP receptor mRNA was expressed in bone marrow cells, indicating a direct effect of BPS on these cells. A recent study has shown that BPS increases eNOS expression in cultured endothelial cells through activation of c-AMP/Protein kinase A signal transduction [19]. Also, earlier studies have shown that eNOS plays essential role in the recruitment of EPCs to the ischemic myocardium [20]. Taken together, administered BPS may act as a potent stimulator of cell mobilization from bone marrow, although further studies are necessary to examine the underlying mechanisms.

In the present study, treatment with BPS significantly attenuated infarct size after myocardial infarction. BPS improved cardiac function and attenuated the development of LV remodeling after acute myocardial infarction, as indicated by increases in LV fractional shortening and maximum dP/dt, and decreases in LVEDP and LVDD. Taken together, BPS may attenuate myocardial infarction through enhancement of neovascularization via modification of bone marrow kinetics. Interestingly, a small fraction of mobilized bone marrow cells expressed cardiac troponin T in the ischemic myocardium in the BPS group, suggesting that BPS may partially contribute to myocardial regeneration after acute myocardial infarction. Earlier studies have demonstrated that BPS has other beneficial effects for ischemic heart disease including anti-thrombotic activity [34], inhibition of reperfusion injury [35], and prevention of coronary spasm [36], and re-stenosis [37]. These findings suggest that administration of BPS may be a promising therapy for acute myocardial infarction.

Granulocyte colony stimulating factor (G-CSF) is currently used agent for mobilization of bone marrow. Infusion of G-CSF after myocardial infarction improves LV function increasing peripheral stem cell fraction [5,38]. A recent clinical trial, however, claimed the G-CSF therapy

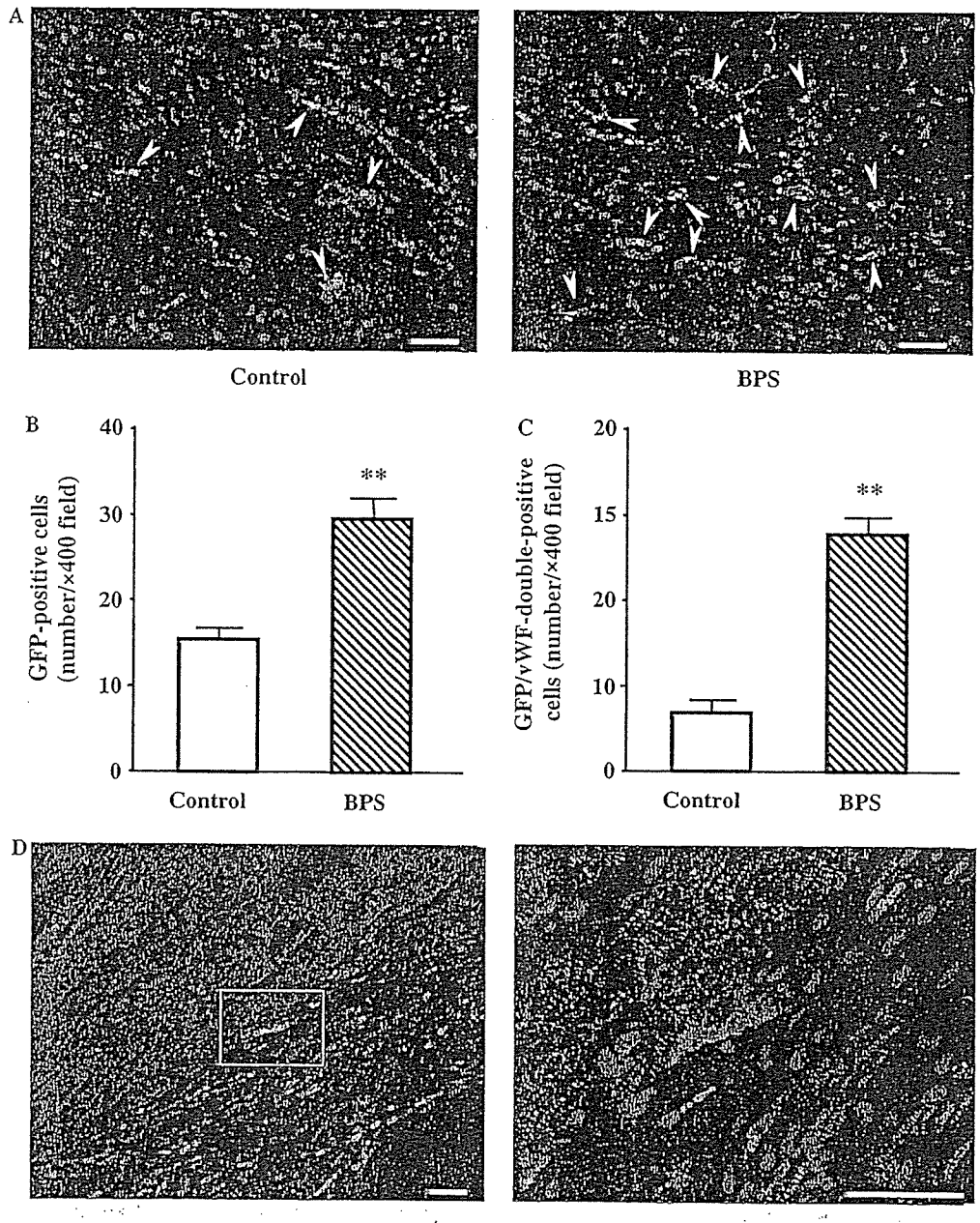

Fig. 4. BPS-induced neovascularization. (A) Representative immunofluorescent images stained with antibodies to von-Willbrand factor (vWF, red) and green fluorescent protein (GFP, green). Nuclei were counterstained with DAPI (blue). (B,C) Semi-quantitative analyses of numbers of GFP-positive cells and GFP-vWF double-positive cells in the peri-infarct area. (D) Representative immunofluorescent image of GFP-positive cells (green) expressing cardiac troponin T (red) observed in the BPS group. Scale bars = 50 μm. Data are expressed as means ± SEM. $^{**}p < 0.01$ vs. Control group.

has serious problem with re-stenosis after recanalization [39]. On the other hand, the safety of BPS has been identified in the treatment of peripheral arterial disease [12,13] and pulmonary arterial hypertension [14,15]. A randomized, controlled clinical trial failed to demonstrate therapeutic potential of prostacyclin for the treatment of severe congestive heart failure [40], which has long discouraged the pursuit of prostacyclin as a therapeutic option for the treatment of acute myocardial infarction. Interestingly, however, double-blinded, randomized, placebo-controlled, large-scale studies showed that treatment with BPS decreased vascular events in patients with peripheral arterial disease [41,42]. Thus, adequate use of BPS for only acute myocardial infarction may have beneficial effects on ischemic myocardium, although further preclinical trials are required to verify the safety and efficacy of BPS.

Conclusion

In summary, administration of BPS improved cardiac structure and function in rats with acute myocardial infarction. This beneficial effect of BPS may be mediated partly by its ability to enhance neovascularization in ischemic myocardium by mobilizing bone marrow cells.

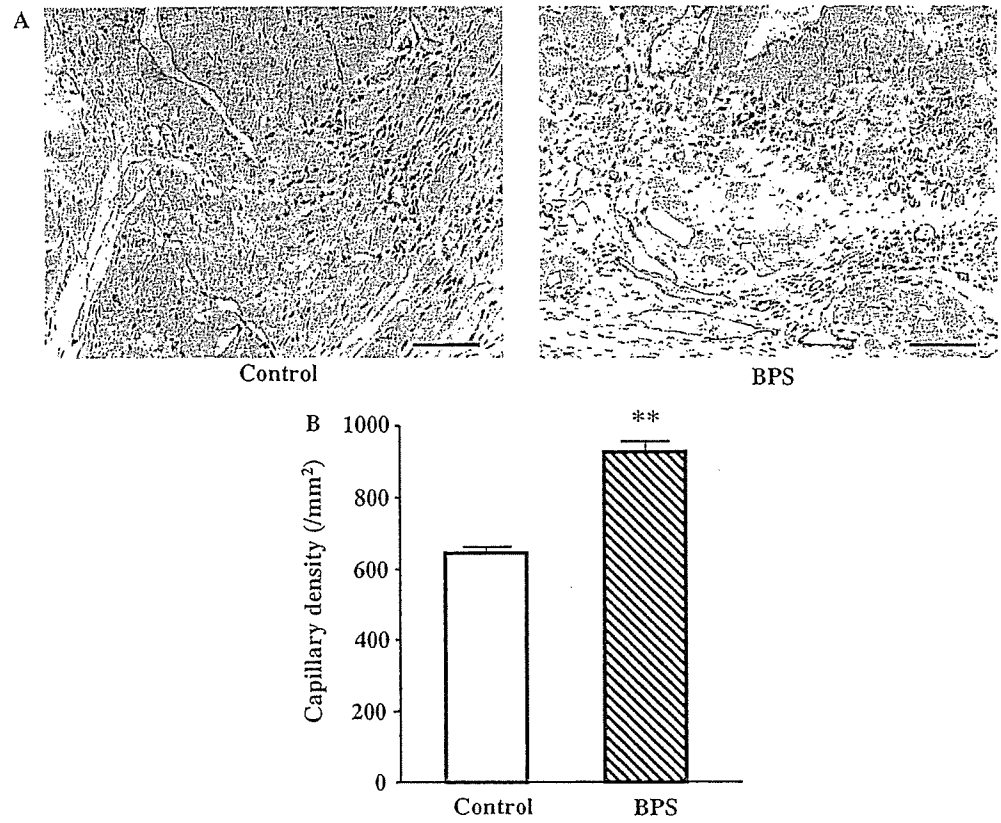

Fig. 5. (A) Representative samples stained with antibody to von Willebrand factor by bright-field DAB. (B) Quantitative analysis of capillary density in peri-infarct area. Administration of BPS increased capillary density by 37%. Scale bars = 50 μm. Data are expressed as means ± SEM. $^{**}p < 0.01$ vs. Control group.

Acknowledgment

This work was supported by research grants for Cardiovascular Disease (16C-6) from the Ministry of Health, Labor and Welfare, and for Japan Vascular Disease Research Foundation.

References

[1] A. Saraste, K. Pulkki, M. Kallajoki, K. Henriksen, M. Parvinen, L.M. Voipio-Pulkki, Apoptosis in human acute myocardial infarction, Circulation 95 (1997) 320–323.
[2] S. Shintani, T. Murohara, H. Ikeda, T. Ueno, T. Honma, A. Katoh, K. Sasaki, T. Shimada, Y. Oike, T. Imaizumi, Mobilization of endothelial progenitor cells in patients with acute myocardial infarction, Circulation 103 (2001) 2776–2779.
[3] D. Orlic, J. Kajstura, S. Chimenti, I. Jakoniuk, S.M. Anderson, B. Li, J. Pickel, R. Mckay, B. Nadal-Ginard, D.M. Bodine, A. Leri, P. Anversa, Bone marrow cells regenerate infarcted myocardium, Nature 410 (2001) 701–705.
[4] H. Oh, S.B. Bradfute, T.D. Gallardo, T. Nakamura, V. Gaussin, Y. Mishina, J. Pocius, L.H. Michael, R.R. Behringer, D.J. Garry, M.L. Entman, M.D. Schneider, Cardiac progenitor cells from adult myocardium: homing, differentiation, and fusion after infarction, Proc. Natl. Acad. Sci. USA 100 (2003) 12313–12318.
[5] D. Orlic, J. Kajstura, S. Chimenti, F. Limana, I. Jakoniuk, F. Quaini, B. Nadal-Ginard, D.M. Bodine, A. Leri, P. Anversa, Mobilized bone marrow cells repair the infarcted heart, improving function and survival, Proc. Natl. Acad. Sci. USA 98 (2001) 10344–10349.
[6] T. Asahara, T. Takahashi, H. Masuda, C. Kalka, D. Chen, H. Iwaguro, Y. Inai, M. Silver, J.M. Isner, VEGF contributes to postnatal neovascularization by mobilizing bone marrow-derived endothelial progenitor cells, EMBO J. 18 (1999) 3964–3972.
[7] T. Murata, T. Murai, T. Kanai, Y. Ogaki, K. Sanai, H. Kanda, S. Sato, N. Kajikawa, T. Umetsu, H. Matsuura, General pharmacology of beraprost sodium, Arzneimittelforschung 39 (1989) 867–876.
[8] T. Akiba, M. Miyazaki, N. Toda, Vasodilator actions of TRK-100, a new prostaglandin I2 analogue, Br. J. Pharmacol. 89 (1986) 703–711.
[9] S. Nishio, H. Matsuura, N. Kanai, Y. Fukatsu, T. Hirano, N. Nishikawa, K. Kameoka, T. Umetsu, The in vitro and ex vivo antiplatelet effect of TRK-100, a stable prostacyclin analog, in several species, Jpn J. Pharmacol. 47 (1988) 1–10.
[10] J.L. Demolis, A. Robert, M. Mouren, C. Funck-Brentano, P. Jaillon, Pharmacokinetics and platelet antiaggregating effects of beraprost, an oral stable prostacyclin analogue, in healthy volunteers, J. Cardiovasc. Pharmacol. 22 (1993) 711–716.
[11] P. Nony, P. Ffrench, P. Girard, S. Delair, S. Azoulay, J.P. Girre, M. Dechavanne, J.P. Boissel, Platelet-aggregation inhibition and hemodynamic effects of beraprost sodium, a new oral prostacyclin derivative: a study in healthy male subjects, Can. J. Physiol. Pharmacol. 74 (1996) 887–893.
[12] M. Murakami, M. Watanabe, H. Furukawa, H. Nakahara, The prostacyclin analogue beraprost sodium prevents occlusion of bypass grafts in patients with lower extremity arterial occlusive disease: a 20-year retrospective study, Ann. Vasc. Surg. 19 (2005) 838–842.
[13] L.T. Cooper, Beraprost for the treatment of intermittent claudication, J. Am. Coll. Cardiol. 41 (2003) 1679–1686.
[14] Y. Okano, T. Yoshioka, A. Shimouchi, T. Satoh, T. Kunieda, Orally active prostacyclin analogue in primary pulmonary hypertension, Lancet 349 (1997) 1365.

[15] N. Nagaya, M. Uematsu, Y. Okano, T. Satoh, S. Kyotani, F. Sakamaki, N. Nakanishi, K. Miyatake, T. Kunieda, Effect of orally active prostacyclin analogue on survival of outpatients with primary pulmonary hypertension, J. Am. Coll. Cardiol. 34 (1999) 1188–1192.
[16] A.M. Lefer, M.L. Ogletree, J.B. Smith, M.J. Silver, K.C. Nicolaou, W.A. Barnette, G.P. Gasic, Prostacyclin: a potentially valuable agent for preserving myocardial tissue in acute myocardial ischemia, Science 200 (1978) 52–54.
[17] B.I. Jugdutt, G.M. Hutchins, B.H. Bulkley, L.C. Becker, Dissimilar effects of prostacyclin, prostaglandin E1, and prostaglandin E2 on myocardial infarct size after coronary occlusion in conscious dogs, Circ. Res. 49 (1981) 685–700.
[18] J.A. Melin, L.C. Becker, Salvage of ischemic myocardium by prostacyclin during experimental myocardial infarction, J. Am. Coll. Cardiol. 2 (1983) 279–286.
[19] K. Niwano, M. Arai, K. Tomaru, T. Uchiyama, Y. Ohyama, M. Kurabayashi, Transcriptional stimulation of the eNOS gene by the stable prostacyclin analogue beraprost is mediated through cAMP-responsive element in vascular endothelial cells: close link between PGI2 signal and NO pathways, Circ. Res. 93 (2003) 523–530.
[20] A. Aicher, C. Heeschen, C. Mildner-Rihm, C. Urbich, C. Ihling, K. Technau-Ihling, A.M. Zeiher, S. Dimmeler, Essential role of endothelial nitric oxide synthase for mobilization of stem and progenitor cells, Nat. Med. 9 (2003) 1370–1376.
[21] T. Nishikimi, K. Uchino, E.D. Frohlich, Effects of α1-adrenergic blockade on intrarenal hemodynamics in heart failure rats, Am. J. Physiol. Regul. Integr. Comp. Physiol. 262 (1998) R198–R203.
[22] P.S. Douglas, N. Reichek, T. Plappert, A. Muhammad, M.G. St John Sutton, Comparison of echocardiographic methods for assessment of left ventricular shortening and wall stress, J. Am. Coll. Cardiol. 9 (1987) 945–951.
[23] Y.W. Chien, R.W. Barbee, A.A. Macphee, E.D. Frohlich, N.C. Trippondo, Increased ANF secretion after volume expansion is preserved in rats with heart failure, Am. J. Physiol. 254 (1988) R185–R191.
[24] T. Ito, A. Suzuki, E. Imai, M. Okabe, M. Hori, Bone marrow is a reservoir of repopulating mesangial cells during glomerular remodeling, J. Am. Soc. Nephrol. 12 (2001) 2625–2635.
[25] P.J. Simpson, R.F. Todd 3rd, J.C. Fantone, J.K. Mickelson, J.D. Griffin, B.R. Lucchesi, Reduction of experimental canine myocardial reperfusion injury by a monoclonal antibody (anti-Mo1, anti-CD11b) that inhibits leukocyte adhesion, J. Clin. Invest. 81 (1988) 624–629.
[26] W.W. Nichols, J. Mehta, T.J. Wargovich, D. Franzini, D. Lawson, Reduced myocardial neutrophil accumulation and infarct size following thromboxane synthetase inhibitor or receptor antagonist, Angiology 40 (1989) 209–221.
[27] M. Kainoh, R. Imai, T. Nakadake, M. Hattori, S. Nishio, Prostacyclin and beraprost sodium as suppressors of activated rat polymorphonuclear leukocytes, Biochem. Pharmacol. 39 (1990) 477–483.
[28] Y. Ueno, Y. Miyauchi, S. Nishio, Beraprost sodium protects occlusion/reperfusion injury in the dog by inhibition of neutrophil migration, Gen. Pharmacol. 25 (1994) 427–432.
[29] A. Kawamoto, T. Tkebuchava, J. Yamaguchi, H. Nishimura, Y.S. Yoon, C. Milliken, S. Uchida, O. Masuo, H. Iwaguro, H. Ma, A. Hanley, M. Silver, M. learney, D.W. Losordo, J.M. Isner, T. Asahara, Intramyocardial transplantation of autologous endothelial progenitor cells for therapeutic neovascularization of myocardial ischemia, Circulation 107 (2003) 461–468.
[30] A. Kawamoto, T. Asahara, D.W. Losordo, Transplantation of endothelial progenitor cells for therapeutic neovascularization, Cardiovasc. Radiat. Med. 3 (2002) 221–225.
[31] A. Weber, I. Pedrosa, A. Kawamoto, N. Himes, J. Munasinghe, T. Asahara, N.M. Rofsky, D.W. Losordo, Magnetic resonance mapping of transplanted endothelial progenitor cells for therapeutic neovascularization in ischemic heart disease, Eur. J. Cardiothorac. Surg. 26 (2004) 137–143.
[32] J. Kajstura, M. Rota, B. Whang, S. Cascapera, T. Hosoda, C. Bearzi, D. Nurzynska, H. Kasahara, E. Zias, M. Bonafe, B. Nadal-Ginard, D. Torella, A. Nascimbene, F. Quaini, K. Urbanek, A. Leri, P. Anversa, Bone marrow cells differentiate in cardiac cell lineages after infarction independently of cell fusion, Circ. Res. 96 (2005) 127–137.
[33] R. Lanza, M.A. Moore, T. Wakayama, A.C. Perry, J.H. Shieh, J. Hendrikx, A. Leri, S. Chimenti, A. Monsen, D. Nurzynska, M.D. West, J. Kajstura, P. Anversa, Regeneration of the infarcted heart with stem cells derived by nuclear transplantation, Circ. Res. 94 (2004) 820–827.
[34] Y. Uchida, T. Hanai, K. Hasegawa, K. Kawamura, T. Oshima, Recanalization of obstructed coronary artery by intracoronary administration of prostacyclin in patients with acute myocardial infarction, Adv. Prostaglandin Thromboxane Leukot. Res. 11 (1983) 377–383.
[35] C.Y. Xiao, A. Hara, Yuhki K, T. Fujino, H. Ma, Y. Okada, O. Takahata, T. Yamada, T. Murata, S. Narumiya, F. Ushikubi, Roles of prostaglandin I(2) and thromboxane A(2) in cardiac ischemia–reperfusion injury: a study using mice lacking their respective receptors, Circulation 104 (2001) 2210–2215.
[36] A. Szczeklik, J. Szczeklik, R. Nizankowski, P. Gluszko, Prostacyclin for unstable angina, N. Engl. J. Med. 303 (1980) 881.
[37] M.L. Knudtson, V.F. Flintoft, D.L. Roth, J.L. Hansen, H.J. Duff, Effect of short-term prostacyclin administration on restenosis after percutaneous transluminal coronary angioplasty, J. Am. Coll. Cardiol. 15 (1990) 691–697.
[38] F. Kuethe, H.R. Figulla, M. Herzau, M. Voth, M. Fritzenwanger, T. Opfermann, K. Pachmann, A. Krack, H.G. Sayer, D. Gottschild, G.S. Werner, Treatment with granulocyte colony-stimulating factor for mobilization of bone marrow cells in patients with acute myocardial infarction, Am. Heart J. 150 (2005) 115.
[39] H.J. Kang, H.S. Kim, S.Y. Zhang, K.W. Park, H.J. Cho, B.K. Koo, Y.J. Kim, D. Soo Lee, D.W. Sohn, K.S. Han, B.H. Oh, M.M. Lee, Y.B. Park, Effects of intracoronary infusion of peripheral blood stem-cells mobilised with granulocyte-colony stimulating factor on left ventricular systolic function and restenosis after coronary stenting in myocardial infarction: the MAGIC cell randomised clinical trial, Lancet 363 (2004) 751–756.
[40] R.M. Califf, K.F. Adams, W.J. McKenna, M. Gheorghiade, B.F. Uretsky, S.E. McNulty, H. Darius, K. Schulman, F. Zannad, E. Handberg-Thurmond, F.E. Harrell Jr., W. Wheeler, J. Soler-Soler, K. Swedberg, A randomized controlled trial of epoprostenol therapy for severe congestive heart failure: The Flolan International Randomized Survival Trial (FIRST), Am. Heart J. 134 (1997) 44–54.
[41] M. Lievre, S. Morand, B. Besse, J.N. Fiessinger, J.P. Boissel, Oral beraprost sodium, a prostaglandin I(2) analogue, for intermittent claudication: a double-blind, randomized, multicenter controlled trial. Beraprost et Claudication Intermittente (BERCI) Research Group, Circulation 102 (2000) 426–431.
[42] E.R. Mohler 3rd, W.R. Hiatt, J.W. Olin, M. Wade, R. Jeffs, A.T. Hirsch, Treatment of intermittent claudication with beraprost sodium, an orally active prostaglandin I2 analogue: a double-blinded, randomized, controlled trial, J. Am. Coll. Cardiol. 41 (2003) 1679–1686.

Japanese Journal of Applied Physics
Vol. 45, No. 6A, 2006, pp. 5301–5306

X-ray Spectra from Weakly Ionized Linear Copper Plasma

Eiichi SATO, Yasuomi HAYASHI, Rudolf GERMER[1], Etsuro TANAKA[2], Hidezo MORI[3], Toshiaki KAWAI[4], Takashi INOUE[5], Akira OGAWA[5], Shigehiro SATO[6], Kazuyoshi TAKAYAMA[7] and Jun ONAGAWA[8]

Department of Physics, Iwate Medical University, 3-16-1 Honchodori, Morioka 020-0015, Japan
[1]*ITP, FHTW FB1 and TU-Berlin, Blankenhainer Str. 9, D 12249 Berlin, Germany*
[2]*Department of Nutritional Science, Faculty of Applied Bio-science, Tokyo University of Agriculture, 1-1-1 Sakuragaoka, Setagaya-ku, Tokyo 156-8502, Japan*
[3]*Department of Cardiac Physiology, National Cardiovascular Center Research Institute, 5-7-1 Fujishirodai, Suita, Osaka 565-8565, Japan*
[4]*Electron Tube Division #2, Hamamatsu Photonics K.K., 314-5 Shimokanzo, Iwata, Shizuoka 438-0193, Japan*
[5]*Department of Neurosurgery, School of Medicine, Iwate Medical University, 19-1 Uchimaru, Morioka 020-8505, Japan*
[6]*Department of Microbiology, School of Medicine, Iwate Medical University, 19-1 Uchimaru, Morioka 020-8505, Japan*
[7]*Shock Wave Research Center, Institute of Fluid Science, Tohoku University, 2-1-1 Katahira, Sendai 980-8577, Japan*
[8]*Department of Applied Physics and Informatics, Faculty of Engineering, Tohoku Gakuin University, 1-13-1 Chuo, Tagajo, Miyagi 985-8537, Japan*

(Received November 20, 2005; accepted April 5, 2006; published online June 8, 2006)

In the plasma flash X-ray generator, a 200 nF condenser is charged up to 50 kV by a power supply, and flash X-rays are produced by the discharging. The X-ray tube is a demountable triode with a trigger electrode, and the turbomolecular pump evacuates air from the tube with a pressure of approximately 1 mPa. Target evaporation leads to the formation of weakly ionized linear plasma, consisting of copper ions and electrons, around the fine target, and intense Kα lines are left using a 10-μm-thick nickel filter. At a charging voltage of 50 kV, the maximum tube voltage was almost equal to the charging voltage of the main condenser, and the peak current was about 16 kA. The K-series characteristic X-rays were clean and intense, and higher harmonic X-rays were observed. The X-ray pulse widths were approximately 300 ns, and the time-integrated X-ray intensity had a value of approximately 1.5 mGy per pulse at 1.0 m from the X-ray source with a charging voltage of 50 kV. [DOI: 10.1143/JJAP.45.5301]

KEYWORDS: linear plasma, X-ray spectra, K-series characteristic X-rays, bremsstrahlung X-rays, higher harmonic X-rays

1. Introduction

In order to produce X-ray lasers, several different methods have been developed, and a discharge capillary[1–3] is very useful to increase the laser pulse energy with increases in the capillary length. However, it is difficult to increase the laser photon energy to 10 keV or beyond.

Using monochrocollimators, synchrotrons produce monochromatic parallel beams, which are fairly similar to monochromatic parallel laser beams, and the beams have been applied to various research project including phase-contrast radiography[4,5] and enhanced K-edge angiography.[6,7] Because there are no X-ray resonators in the high-photon-energy region, new methods for increasing coherence will be desired in the future.

To apply flash X-ray generators to biomedicine, several different generators[8–13] have been developed, and plasma X-ray generators[14–17] are useful for producing clean characteristic X-rays in the low-photon-energy region of less than 10 keV. By forming weakly ionized linear plasma using rod targets, intense K-series characteristic X-rays are observed from the axial direction of the linear plasmas of nickel and copper, since the bremsstrahlung X-rays are absorbed effectively by the linear plasma. We are therefore very interested in the X-ray spectra produced by increasing the charging voltage in the high photon energy region beyond Kβ energies.

In this paper, we describe a recent table-top plasma flash X-ray generator utilizing a rod target triode, used to perform a preliminary experiment for generating clean K-series characteristic X-rays and their higher harmonic hard X-rays by forming a linear copper plasma cloud around a fine target.

2. Generator

Figure 1 shows a block diagram of the high-intensity plasma flash X-ray generator. This generator consists of the following essential components: a high-voltage power supply, a high-voltage condenser with a capacity of approximately 200 nF, a turbomolecular pump, a krytron pulse generator as a trigger device, and a flash X-ray tube. The high-voltage main condenser is charged to 50 kV by the power supply, and electric charges in the condenser are discharged to the tube after triggering the cathode electrode with the trigger device. The plasma flash X-rays are then produced.

The X-ray tube is a demountable cold-cathode triode that is connected to the turbomolecular pump with a pressure of approximately 1 mPa. This tube consists of the following major parts: a hollow cylindrical carbon cathode with a bore diameter of 10.0 mm, a brass focusing electrode, a trigger electrode made from copper wire, a stainless steel vacuum chamber, a nylon insulator, a poly(ethylene terephthalate) (Mylar) X-ray window 0.25 mm in thickness, and a rod-shaped copper target 3.0 mm in diameter with a tip angle of 60°. The distance between the target and cathode electrodes is approximately 20 mm, and the trigger electrode is set in the cathode electrode. As electron beams from the cathode electrode are roughly converged to the target by the focusing electrode, evaporation leads to the formation of a weakly ionized linear plasma,[18] consisting of copper ions and electrons, around the fine target.

In the linear plasma, bremsstrahlung photons with energies higher than the K-absorption edge are effectively absorbed and are converted into fluorescent X-rays. The plasma then transmits the fluorescent rays easily, and bremsstrahlung rays with energies lower than the K-edge

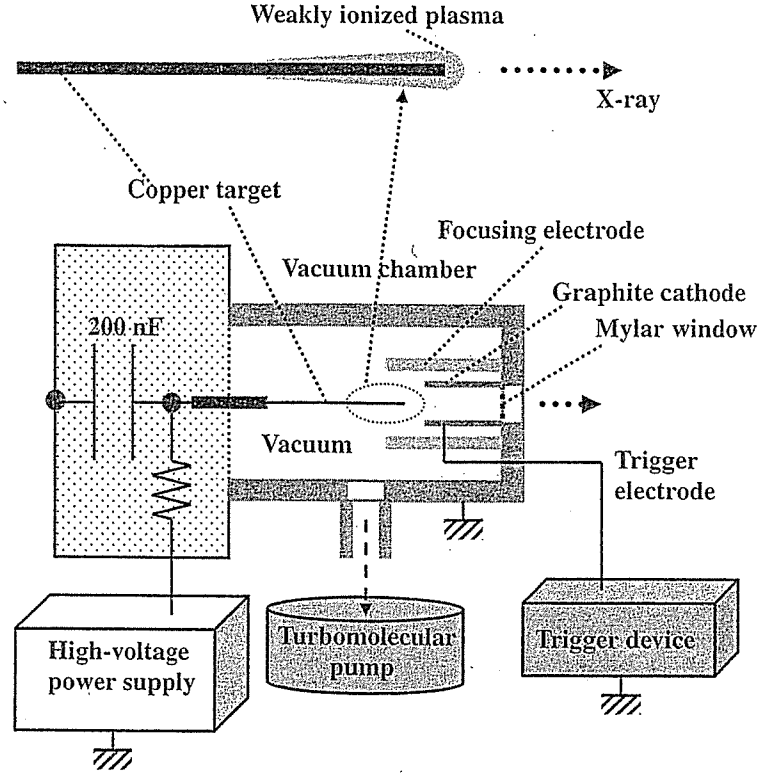

Fig. 1. Block diagram including the electric circuit of the plasma flash X-ray generator.

are also absorbed by the plasma. In addition, because bremsstrahlung rays are not emitted in the opposite direction to that of electron trajectory, intense characteristic X-rays are generated from the plasma-axial direction.

3. Characteristics

3.1 Tube voltage and current

Tube voltage and current were measured by a high-voltage divider with an input impedance of 1 GΩ and a current transformer, respectively. The withstand voltage of the divider is approximately 60 kV, and the measurable current of the transformer ranges from 1 A to 100 kA. Figure 2 shows the time relation between the tube voltage and current. At the indicated charging voltages, they roughly displayed damped oscillations. When the charging voltage was increased, both the maximum tube voltage and current increased. At a charging voltage of 50 kV, the maximum tube voltage was almost equal to the charging voltage of the main condenser, and the maximum tube current was approximately 16 kA.

3.2 X-ray output

X-ray output pulse was detected using a combination of a plastic scintillator and a photomultiplier (Fig. 3). The X-ray pulse height substantially increased with corresponding increases in the charging voltage. The rise time increased with increasing the voltage because the K-series characteristic X-rays were produced with tube voltages beyond the critical excitation voltage of 8.9 kV. The X-ray pulse widths were about 300 ns, and the time-integrated X-ray intensity per pulse measured by a thermoluminescence dosimeter (Kyokko TLD Reader 1500 having MSO-S elements without energy compensation) had a value of approximately 1.5 mGy at 1.0 m from the X-ray source with a charging voltage of 50 kV. The TLD reader has a wide measurable range of from 1 μSv to 100 Sv.

3.3 X-ray source

In order to roughly observe images of the plasma X-ray source in the detector plane, we employed a pinhole camera with a hole diameter of 100 μm without using a filter (Fig. 4). When the charging voltage was increased, the plasma X-ray source grew, and both spot dimension and intensity increased. Because the X-ray intensity is the highest at the center of the spot, both the dimension and intensity decreased according to both increases in the thickness of a filter for absorbing X-rays and decreases in the pinhole diameter.

3.4 X-ray spectra

X-ray spectra from the plasma source were measured by a transmission-type spectrometer with a lithium fluoride curved crystal 0.5 mm in thickness. The spectra were taken by a computed radiography (CR) system[19] (Konica Minolta, Regius 150) with a wide dynamic range beyond five figures for measuring X-ray intensity, and relative X-ray intensity was calculated from Dicom digital data. Subsequently, the relative X-ray intensity as a function of the data was calibrated using a conventional X-ray generator, and we confirmed that the intensity was proportional to the exposure time. Figure 5 shows measured spectra from the copper target at the indicated conditions. In fact, we observed clean K lines, and Kα lines were left by absorbing Kβ lines using a 10-μm-thick nickel filter. When the charging voltage was increased, the characteristic X-ray intensity substantially increased. In particular, we confirmed the irradiation of

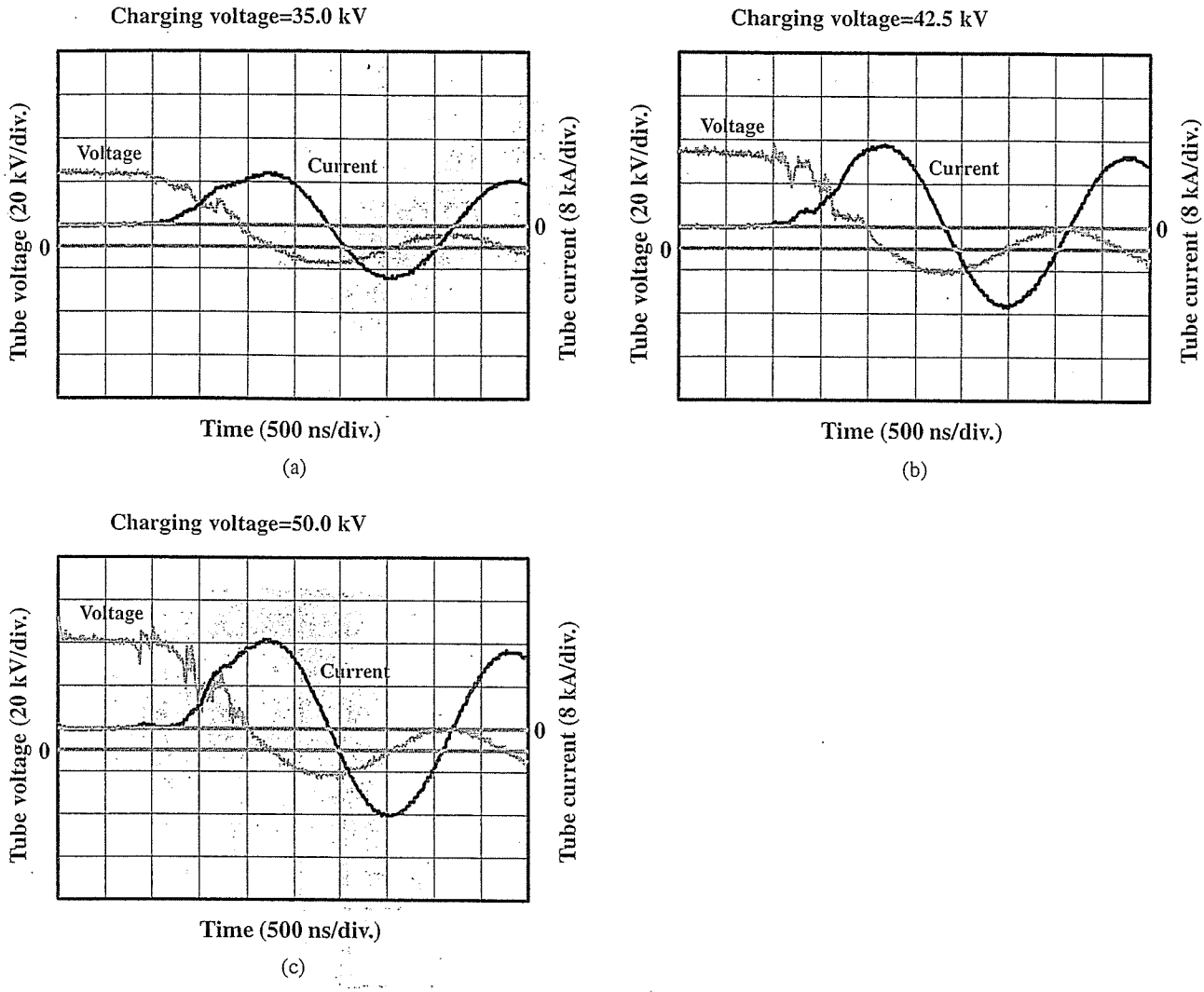

Fig. 2. Tube voltages and currents with a charging voltage of (a) 35.0, (b) 42.5, and (b) 50.0 kV.

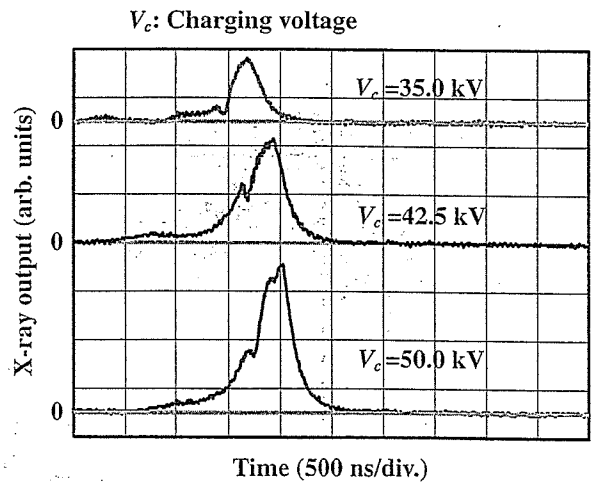

Fig. 3. X-ray outputs at the indicated conditions.

the second and fourth harmonic X-rays of the fundamental K-series characteristic X-rays from copper target. The X-ray intensities of the harmonics increased with increases in the charging voltage, and the harmonic bremsstrahlung rays survived due to the X-ray resonation in the plasma.

4. Radiography

The plasma radiography was performed by the CR system using the filter. The charging voltage and the distance between the X-ray source and imaging plate were 50 kV and 1.2 m, respectively. First, rough measurements of spatial resolution were made using wires. Figure 6 shows radiograms of tungsten wires coiled around pipes made of poly(methyl methacrylate) (PMMA). Although the image contrast decreased somewhat with decreases in the wire diameter, due to blurring of the image caused by the sampling pitch of 87.5 μm, a 50-μm-diameter wire could be observed.

Figure 7 shows a radiogram of plastic bullets falling into a polypropylene beaker from a plastic test tube. Because the X-ray duration was about 0.5 μs, the stop-motion image of bullets could be obtained. Next, a radiogram of a vertebra is shown in Fig. 8, and fine structures in the vertebra were observed. Finally, Fig. 9 shows an angiogram of a rabbit ear; iodine-based microspheres of 15 μm in diameter were used, and fine blood vessels of about 100 μm were visible.

5. Conclusions and Outlook

We obtained fairly intense and clean K lines from a weakly ionized linear copper plasma, and Kα lines were left

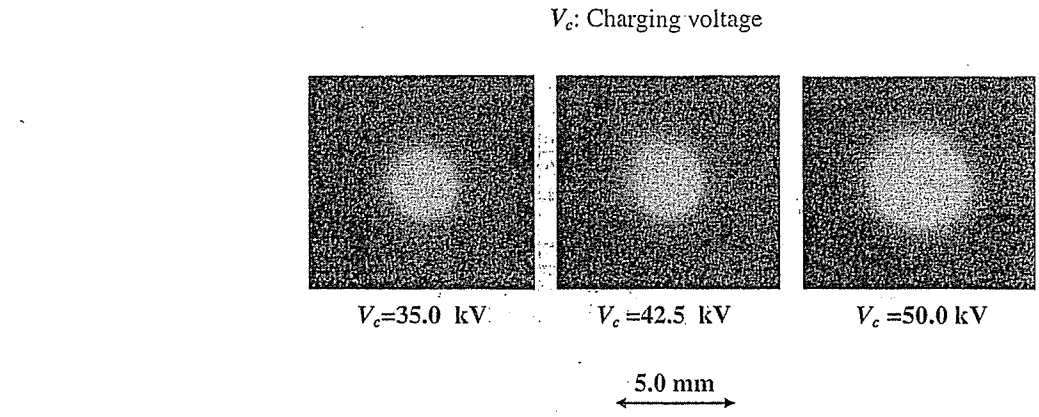

Fig. 4. Images of the plasma X-ray source.

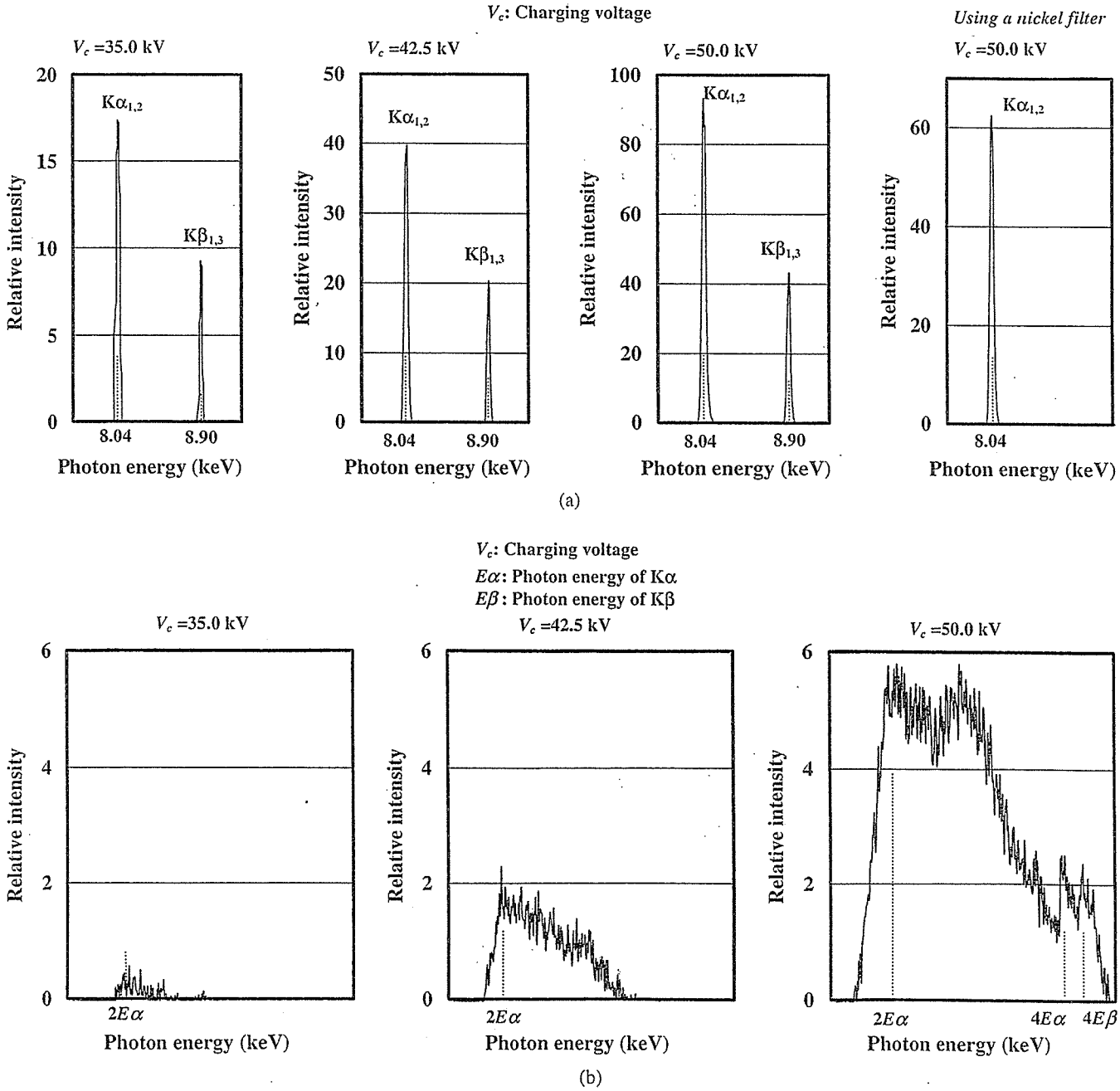

Fig. 5. X-ray spectra from weakly ionized copper plasma at the indicated conditions. (a) characteristic X-rays and (b) higher harmonic X-rays.

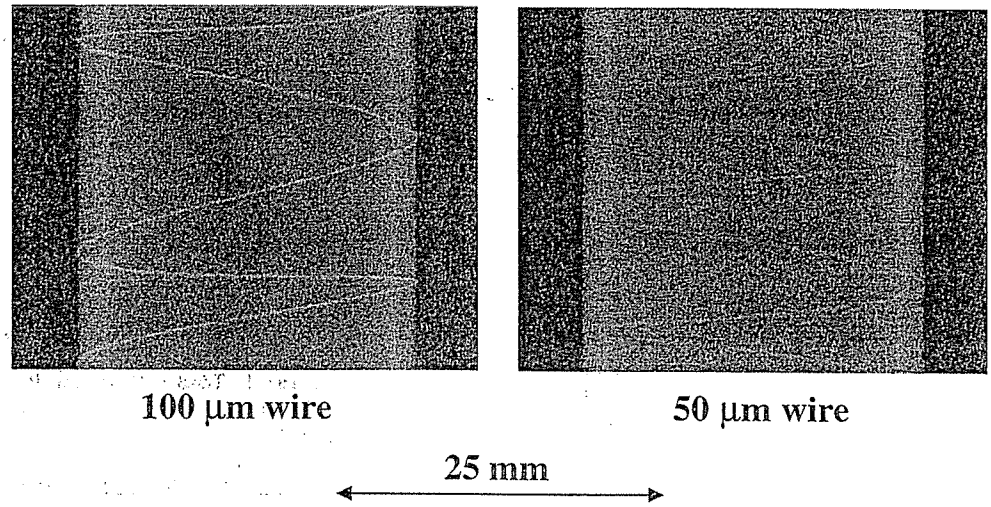

Fig. 6. Radiograms of tungsten wires coiled around PMMA pipes.

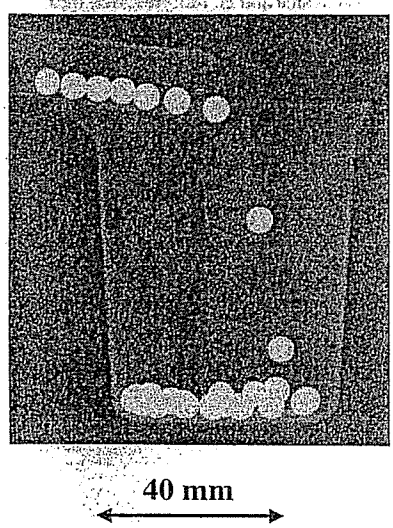

Fig. 7. Radiogram of plastic bullets falling into polypropylene beaker from a plastic test tube.

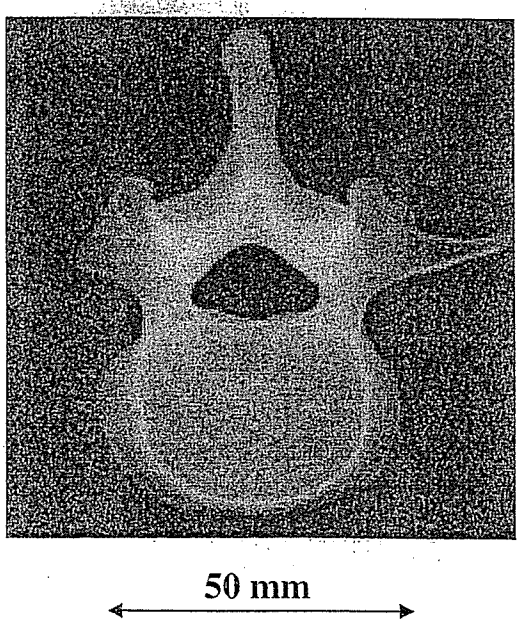

Fig. 8. Radiogram of a vertebra.

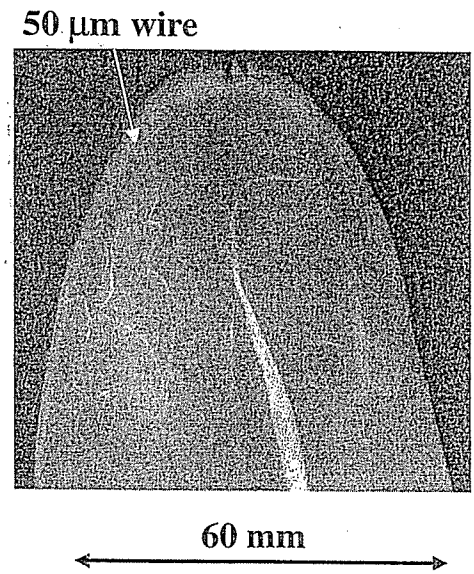

Fig. 9. Angiogram of a rabbit ear.

by the nickel filter. Both the characteristic and the harmonic X-ray intensities substantially increased with increasing the charging voltage.

In cases where weakly ionized linear plasma is employed, intense and clean K-series characteristic X-rays can be obtained. However, it is not easy to produce high-photon-energy K-series characteristic X-rays because the linear plasma transmits high-photon-energy bremsstrahlung X-rays; the effective thickness of a monochromatic metal filter increases with increases in the atomic number. Therefore, high-photon-energy plasma flash X-ray generators utilizing the angle dependence of bremsstrahlung X-rays are very useful to produce K photons of molybdenum, silver, cerium, tantalum, and tungsten. In particular, Kα rays of tantalum and tungsten are useful for performing enhanced K-edge angiography using gadolinium contrast media, and cerium K rays can be employed to perform iodine K-edge angiography.

In this research, we obtained sufficient characteristic X-ray intensity per pulse for CR radiography, and the